minerals

MDPI

Article

Timing and Provenance Transition of the Neoproterozoic Wuling Unconformity and Xihuangshan Unconformity of the Yangtze Block: Responses to Peripheral Orogenic Events

Dinghua Li [1,2,3], Zhenning Yang [1,4,*], Yu Liu [1,5], Kunguang Yang [1,2], Dehai Wu [3] and Pingting Cai [3]

1 School of Earth Sciences, China University of Geosciences Wuhan, Wuhan 430074, China; lidinghua001@163.com (D.L.); yliu25@gzu.edu.cn (Y.L.); yangkunguang@163.com (K.Y.)
2 Key Laboratory of Tectonics and Petroleum Resources, Ministry of Education, China University of Geosciences Wuhan, Wuhan 430074, China
3 Key Laboratory of Ionic Rare Earth Resources and Environment, Ministry of Natural Resources, Jiangxi College of Applied Technology, Ganzhou 341000, China; dehaiwu@163.com (D.W.); cpt0327@163.com (P.C.)
4 Hebei Key Laboratory of Strategic Critical Mineral Resources, Hebei GEO University, Shijiazhuang 050031, China
5 College of Resources and Environmental Engineering, Guizhou University, Guiyang 550025, China
* Correspondence: znyang@hgu.edu.cn; Tel.: +86-27-6788-3596

Abstract: Middle Neoproterozoic sedimentary strata are widely distributed on the periphery of the Yangtze Block. In the western Jiangnan Orogen, they are divided into the Lengjiaxi and Banxi groups by the "Wuling unconformity", and the Banxi Group is further divided into the Madiyi Formation and Wuqiangxi Formation by the "Xihuangshan unconformity". However, the timing and tectonic significance of the Wuling and Xihuangshan unconformities remain unclear, which hampers our understanding of the Precambrian tectonic evolution of the Yangtze Block. Zircon U–Pb dating and Lu–Hf isotopic analysis were performed on the sedimentary rocks above and below the two unconformity boundaries in the western Jiangnan Orogen. These data were used to trace sedimentary provenance and provide new insights into the basin evolution and tectonic significance of the unconformities. Combined with previous studies, the Wuling unconformity is bracketed to have formed between ~830 and 813 Ma, and the provenance of the sediments above the unconformity remained unchanged. The detrital zircons from the upper parts of the Lengjiaxi Group and lower parts of the Banxi Group show the primary peak ages of 800–1000 Ma, 1.0–1.30 Ga, 1.40–1.90 Ga, and 2.30–2.60 Ga, and the provenance mainly derived from the southwestern margin of the Yangtze Block, Cathaysia Block, and Jiangnan Orogen. The provenance from the Cathaysia Block occurred in the upper part of the Lengjiaxi Group, indicating that the Yangtze Block and Cathaysia Block merged in the western Jiangnan Orogen earlier than the formation time of the Wuling unconformity (~830–813 Ma) and the collisional time in the eastern Jiangnan Orogen (~820–800 Ma). Thus, the collision between the Yangtze and Cathaysia blocks may have undergone a scissor-like closure process from west to east. The formation time of the Xihuangshan unconformity was at ~800–779 Ma. The field contact relationships changed from an angular unconformity to a disconformity and then to conformity, from north to south, indicating that the Xihuangshan unconformity was controlled by tectonic movement in the north. The provenance of the sedimentary strata changed above the Xihuangshan unconformity. The detrital zircon age peaks of the upper Banxi Group are 755–1000 Ma, 1.90–2.10 Ga, and 2.35–2.70 Ga, and the detritus were derived from the northern margin of the Yangtze Block and the Jiangnan Orogen. This unconformity is coeval with that of the ~800–780 Ma collisional orogeny at the northern and northwestern margins of the Yangtze Block. Thus, the Xihuangshan unconformity is likely a response to the collision orogeny in the northern and northwestern margins of the Yangtze Block and induces the transition of sedimentary provenance.

Keywords: western Jiangnan Orogen; Wuling unconformity; Xihuangshan unconformity; detrital zircon U−Pb dating; Lu−Hf isotopes; Rodinia supercontinent

check for updates

Citation: Li, D.; Yang, Z.; Liu, Y.; Yang, K.; Wu, D.; Cai, P. Timing and Provenance Transition of the Neoproterozoic Wuling Unconformity and Xihuangshan Unconformity of the Yangtze Block: Responses to Peripheral Orogenic Events. *Minerals* **2022**, *12*, 596. https://doi.org/10.3390/min12050596

Academic Editor: Yamirka Rojas-Agramonte

Received: 23 February 2022
Accepted: 29 April 2022
Published: 7 May 2022

Publisher's Note: MDPI stays neutral with regard to jurisdictional claims in published maps and institutional affiliations.

Copyright: © 2022 by the authors. Licensee MDPI, Basel, Switzerland. This article is an open access article distributed under the terms and conditions of the Creative Commons Attribution (CC BY) license (https://creativecommons.org/licenses/by/4.0/).

1. Introduction

The Rodinia supercontinent is regarded as the assembly of the main continents during the late Mesoproterozoic to early Neoproterozoic [1–3]. Its formation and breakup have been widely discussed over the past decades [2,4–11]. The South China Block, formed by the amalgamation of the Yangtze and Cathysia blocks, is considered an integral part of the Rodinia supercontinent (Figure 1a) [2,4,12–14]. However, the Neoproterozoic evolution of the Yangtze Block is still highly controversial, and three different tectonic models have been proposed: the plume-rift model [15–18], slab-arc model [19–21], and plate-rift model [13,22].

A matter of significant debate among these competing models is the timing of the amalgamation of the Yangtze and Cathaysia blocks along the Jiangnan Orogen (or the Sibao or Jinning Orogen by different authors; Figure 1b) [23]. Some scholars believe that the collision between the Yangtze and Cathaysia blocks occurred along the Jiangnan Orogen during 1000–880 Ma [2,4,15,24–26]. Other researchers have noted that this splicing occurred at ~860–800 Ma [19,22,27–32]. Different opinions exist regarding splicing styles such as southward subduction [33], northward subduction [21,34–36], divergent double subduction [29,37,38], and scissor closure [17,35].

Over the past two decades, much attention has been focused on the petro genesis, and tectonic setting of Neoproterozoic igneous rocks in the Jiangnan Orogen (e.g., [6,7,13,15,21,22,24–26,29–32,34,35,37]), whereas less attention has been given to the middle Neoproterozoic unconformities (i.e., Wuling and Xihuangshan unconformities) and associated sedimentary strata (e.g., [18,39,40]). The middle Neoproterozoic Wuling unconformity is generally considered a sign of the collision and merging of the Yangtze and Cathaysia blocks at the southeastern edge of the Yangtze Block (e.g., [23]). Above the "Wuling unconformity", there is another Neoproterozoic unconformity called the "Xihuangshan unconformity". The Neoproterozoic sedimentary strata (Lengjiaxi and Banxi groups) across these two unconformities record peripheral orogenic events and are crucial for understanding the Neoproterozoic tectonic evolution of the Yangtze Block. Some studies have found that the upper and lower strata across the Wuling unconformity have similar provenance [18,39,40], whereas others have proposed the existence of a provenance transition between the Banxi and Lengjiaxi groups across the Wuling unconformity in this region [41–43]. However, the formation age, distribution range, and tectonic significance of the Xihuangshan unconformity, as well as the provenance of the strata across the Xihuangshan unconformity, are still poorly understood.

In this study, middle Neoproterozoic clastic rocks above and below the Wuling and Xihuangshan unconformities in the Guzhang and Zhijiang areas of the Hunan Province in the western Jiangnan Orogen were observed. Detailed detrital zircon U–Pb dating and Hf isotopic analysis were performed to provide new insights into the tectonic significance of these two unconformities in the western Jiangnan Orogen and their implications for the Neoproterozoic orogenic event around the Yangtze Block.

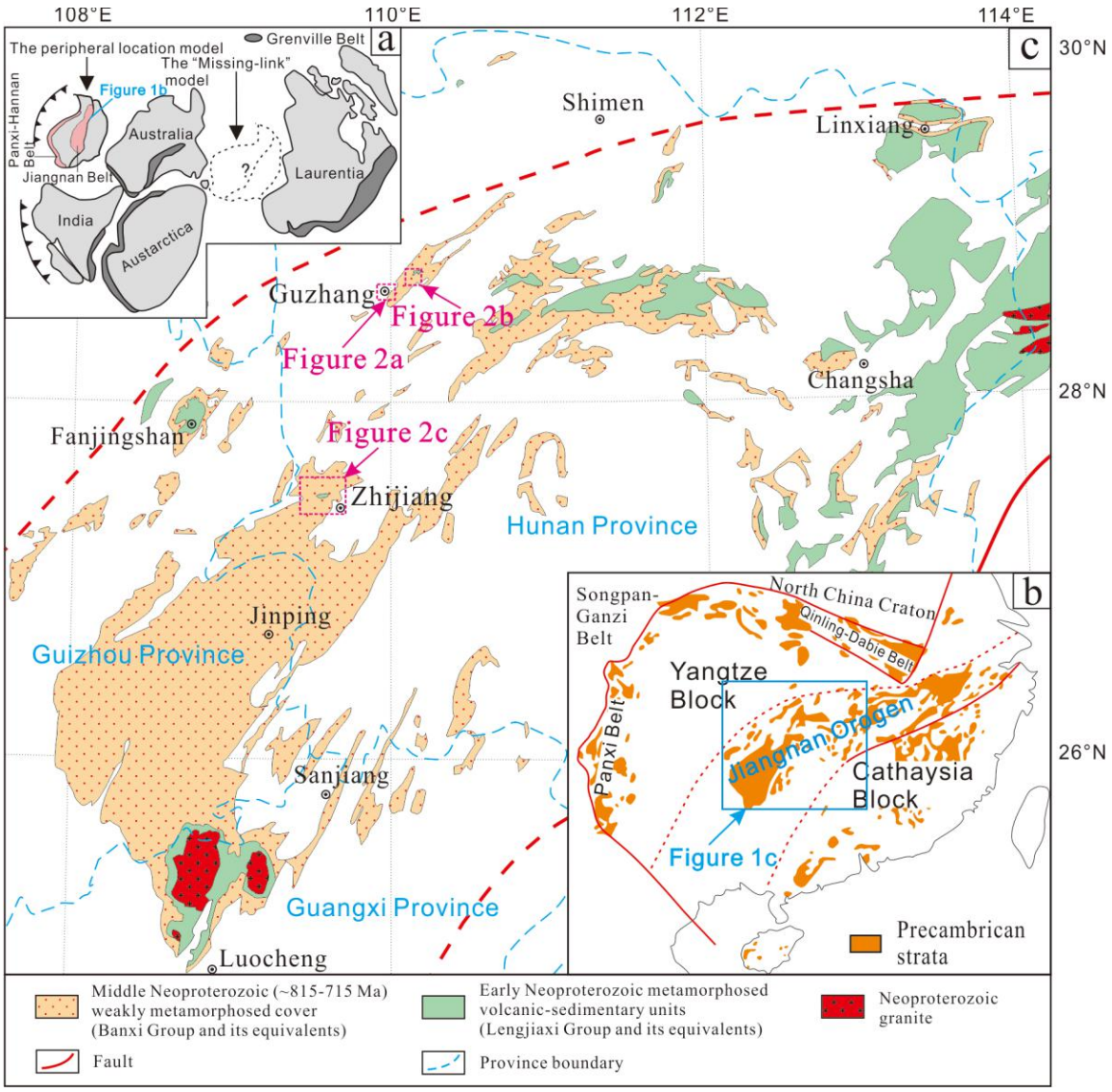


Figure 1. (**a**) Position of the South China Block in the reconstruction of Rodinia (modified after [44]). (**b**) Geological map showing the distribution of Precambrian strata of South China. The Jiangnan Orogen separated the Yangtze Block in the northwest from the Cathaysia Block in the southeast (modified after [42,45]). (**c**) Simplified geological map of the Western Jiangnan Orogen (WJO) (revised after [46–48]).

2. Geological Setting and Sampling

2.1. Geological Setting

It is believed that the South China Block was formed by the merger of the Yangtze Block in the northwest and the Cathaysia Block in the southeast during the Neoproterozoic (Figure 1b; [10,27,38]). It is separated from the North China Craton by the Qinling-Dabie Belt to the north and from Tibet by the Songpan-Ganzi Belt and Panxi Belt to the west [49]. The Precambrian basement of the Yangtze Block is mainly composed of Proterozoic rocks with scarce Archean outcrops [10]. The Archean to Paleoproterozoic rock assemblages of the Yangtze Block mainly contain the Dahongshan, Dongchuan, and Hekou groups on the southwestern margin of the Yangtze Block, the Kongling Complex, Yudongzi Group, and Houhe Complex on the northern margin of the Yangtze Block, and the Huangtuling Complex in the Qinling-Dabie Belt [10,42,50]. Mesoproterozoic rock outcrops such as the Tianli schist, Kunyang Group, and Huili Group are mainly distributed in the south-

eastern and southwestern margins of the Yangtze Block [50]. Contrary to the sporadic exposure of pre-Neoproterozoic rocks in the Yangtze Block, the early-middle Neoproterozoic (1000–720 Ma) metamorphosed volcanic sedimentary units and magmatic rocks are widely distributed around the Yangtze Block [10,51]. Neoproterozoic metamorphic rocks are also widely exposed in the Cathaysia Block and are primarily affected by greenschist facies metamorphism [50].

The Jiangnan Orogen is located along the southeastern margin of the Yangtze Block, with a length of 1500 km in an east–west direction. It is mainly composed of Neoproterozoic sedimentary strata and magmatic rocks [23]. The Neoproterozoic sedimentary strata in the western Jiangnan Orogen are divided into two parts by the Wuling unconformity. The basement sequence below the Wuling unconformity includes phyllite, slate, sandstone, and siltstone with a small number of tholeiitic lavas and volcaniclastic interlayers, called the Lengjiaxi Group, Fanjingshan Group, and Sibao Group [46–48]. The overlying weakly metamorphosed Banxi, Xiajiang, and Danzhou groups are mainly composed of sandstone, slate, conglomerate, marl, carbonate, shale, and volcaniclastic rocks [16,23]. Available geochronological studies suggest that the Banxi Group was formed at ~815–715 Ma [44,52–55] and was separated into the Madiyi and Wuqiangxi formations from the bottom to the top by the Xihuangshan unconformity (Figure 2; [56]).

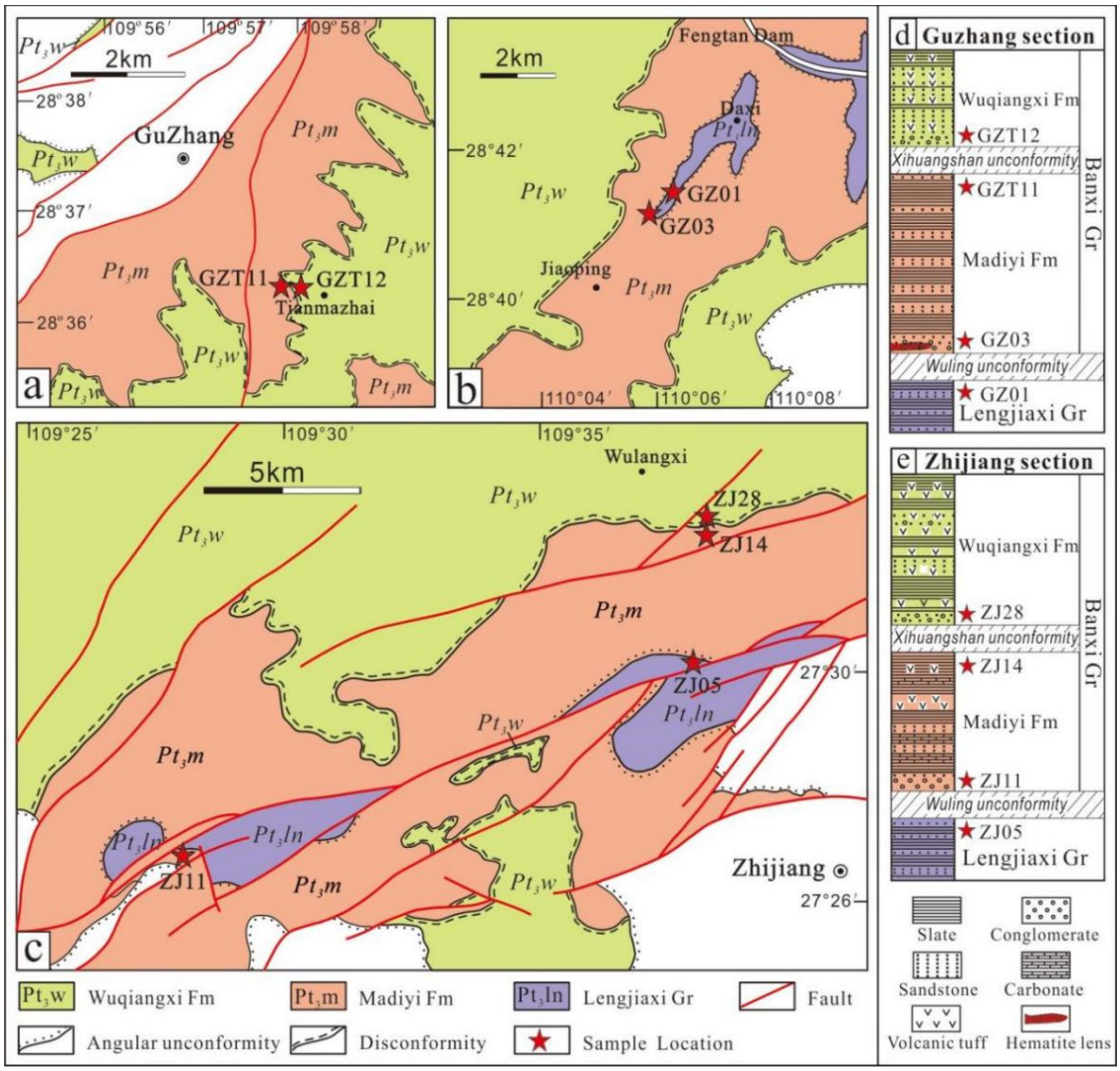


Figure 2. (**a**,**b**) Geological map of the sample locations in Guzhang area; (**c**) geological map of the sample locations in Zhijiang area; (**d**) stratigraphic section in Guzhang area and (**e**) Zhijiang area. (revised after [48,57]). Abbreviations: Gr—Group; Fm—Formation.

2.2. Sample Descriptions

Based on detailed geological fieldwork, a total of eight samples were selected across the Wuling and Xihuangshan unconformities in the Zhijiang and Guzhang regions (Hunan Province, China) for zircon U−Pb dating and Hf isotopic analysis. Sample locations are shown in Figures 1c and 2 and Table 1.

Table 1. Sampling locations and the petrological features for metasedimentary rocks from the WJO.

Sample	GPS	Rock Type	Compositions
GZ01	N 28°41′25.5″, E 110°06′17.5″	Fine-grained lithic sandstone	45% quartz, 35% debris, 10% feldspar, 5% sericite, 5% cement
GZ03	N 28°41′05.6″, E 110°05′51.3″	Fine-grained iron lithic sandstone	38% quartz, 35% debris, 10% sericite, 4% feldspar, 10% ferruginous cement, 3% matrix
GZT11	N 28°36′18.9″, E 109°57′56.2″	Fine-grained lithic sandstone	50% quartz, 40% debris, 5% feldspar, 5% sericite, 5% cement
GZT12	N 28°36′18.3″, E 109°57′57.6″	Pebbly lithic quartz sandstone	70% quartz, 17% debris, 3% feldspar, 5% sericite, 5% calcareous cement
ZJ05	N 27°30′18.4″, E 109°38′12.8″	Feldspar lithic sandstone	45% quartz, 30% debris, 10% feldspar, 10% calcareous cement, 5% matrix
ZJ11	N 27°26′38.4″, E 109°28′17.4″	Medium-grained lithic sandstone	40% quartz, 36% debris, 5% sericite, 4% feldspar, 10% ferruginous cement, 5% matrix
ZJ14	N 27°32′48.8″, E 109°37′53.4″	Silty slate	30% quartz, 15% sericite, 5% ferruginous cement, 50% argillaceous
ZJ28	N 27°32′48.8″, E 109°37′53.4″	Sandy conglomerate	80% quartz, 4% feldspar, 6% debris, 7% cement, 3% matrix

Samples GZ01 and ZJ05 were gray-green fine-grained lithic sandstone and medium-grained feldspathic lithic sandstone, respectively, taken from the upper part of the Lengjixi Group (Figure 3a,b). Samples GZ03 and ZJ11 were fine-grained lithic sandstone and medium-grained lithic sandstones obtained from the bottom of the Madiyi Formation (Figure 3c,d). Samples GZT11 and ZJ14 were fine-grained lithic sandstone (Figure 4e) and silty slate collected from the top of the Madiyi Formation beneath the Xihuangshan unconformity (Figure 4f). Samples GZT12 and ZJ28 were gray-white pebbly lithic quartz sandstone and gray sandy conglomerate sampled from the bottom of the Wuqiangxi Formation above the Xihuangshan unconformity (Figures 3e,f and 4g,h). The GPS locations and petrological features of the samples are presented in Table 1.

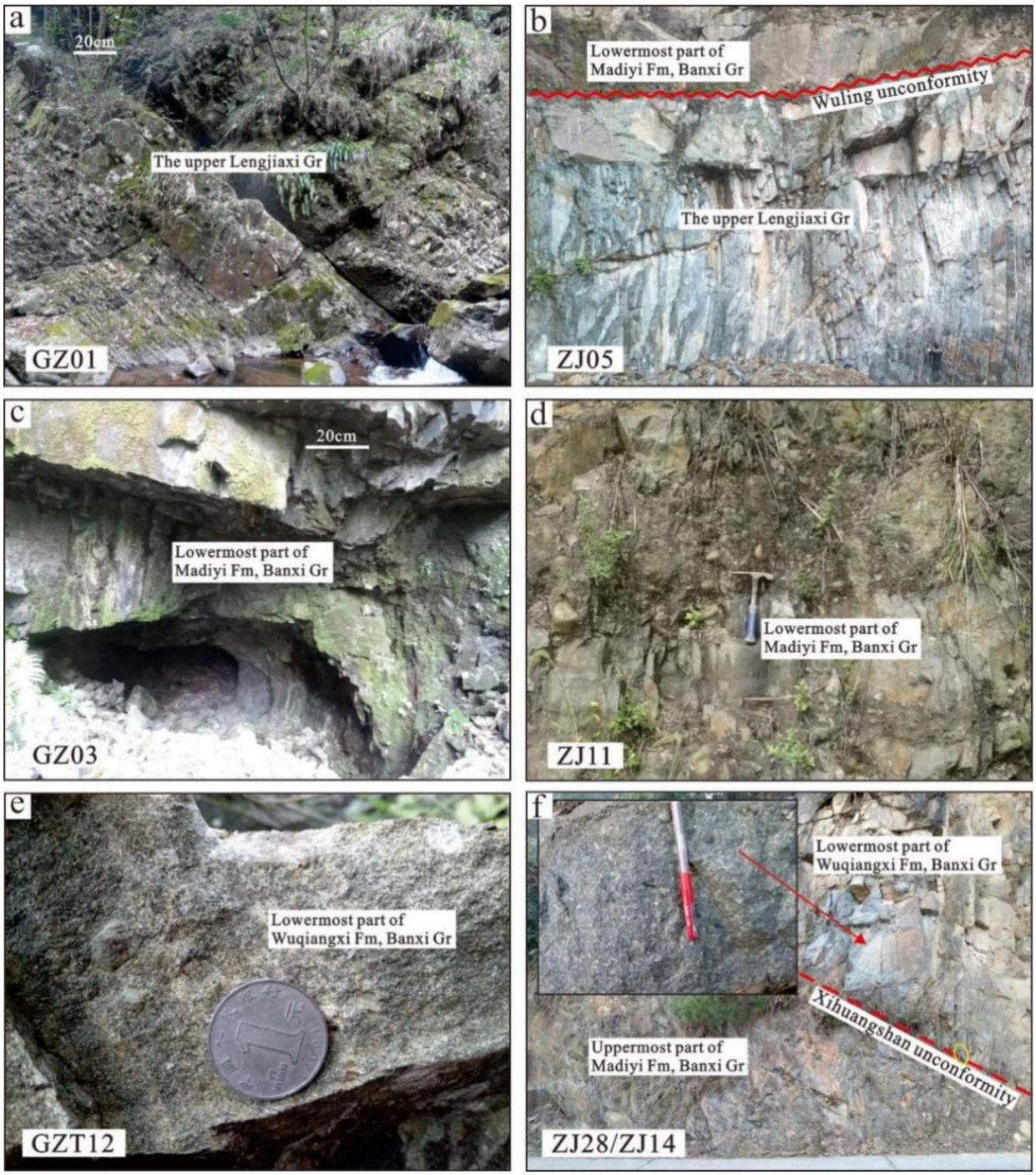


Figure 3. Field photographs showing the outcrops of the Lengjiaxi and Banxi groups in the Guzhang and Zhijiang areas. (**a**) Fine-grained lithic sandstone at the upper part of the Lengjiaxi Group in Guzhang County; (**b**) Wuling angular unconformity between the underlying Lengjiaxi Group and overlying Banxi Group in Zhijiang County; (**c**) fine-grained lithic sandstone at the the bottom of the Madiyi Formation in Guzhang County; (**d**) conglomerate interbedded with medium-grained lithic sandstone at the bottom of the Madiyi Formation in Zhijiang County; (**e**) pebbly lithic quartz sandstone at the the bottom of the Wuqiangxi Formation in Guzhang County; (**f**) sandy conglomerate at the bottom of the Wuqiangxi Formation above the Xihuangshan unconformity.

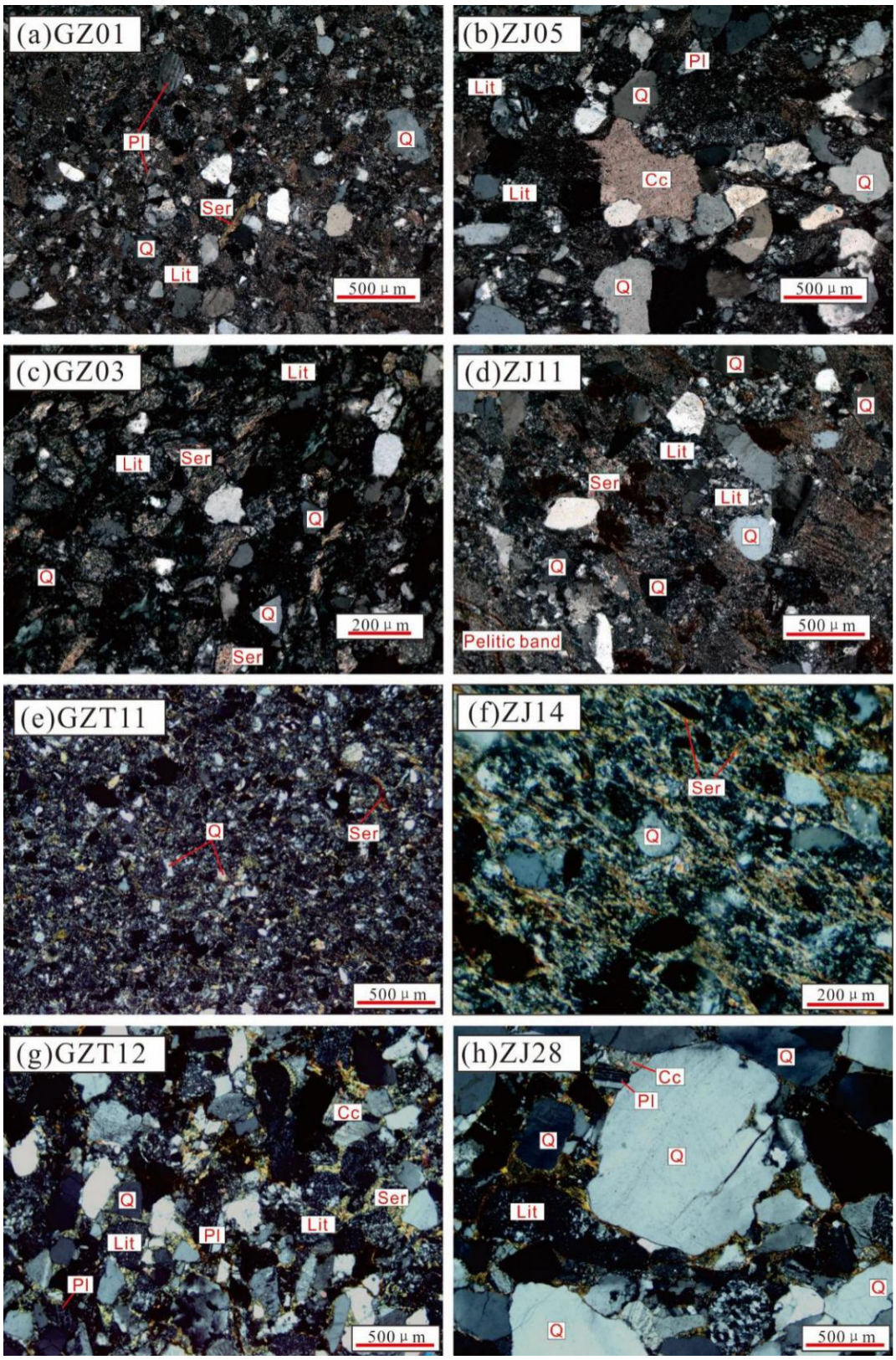


Figure 4. Photomicrographs of samples analyzed in this study. (**a**) Fine-grained lithic sandstone; (**b**) medium-grained feldspathic lithic sandstone; (**c**) fine-grained lithic sandstone; (**d**) medium-grained lithic sandstones; (**e**) fine-grained lithic sandstone; (**f**) silty slate; (**g**) pebbly lithic quartz sandstone; (**h**) sandy conglomerate. Q—quartz; Pl—plagioclase; Ser—sericite; Lit—lithic clast; Cc—calcite.

3. Analytical Methods

3.1. Zircon LA−ICP−MS U−Pb Dating

Zircon grains were obtained from the samples by heavy-liquid and magnetic separation techniques and then mounted in epoxy and polished. The external and internal structures of the zircons were documented by transmitted and reflected light photomicrographs and Cathodoluminescence (CL) images, which were used to select target sites for U-Pb dating and Hf isotopic analysis. Zircon U-Pb dating analysis was performed by LA−ICP−MS at the State Key Laboratory of Geological Processes and Mineral Resources, China University of Geosciences, Wuhan (SKLGPMR−CUG). A GeoLas 2005 excimer ArF laser-ablation system and Agilent 7500a ICP−MS instrument were combined for the experiments. The detailed instrumental setting, operating procedures, and offline data reduction were described by Liu et al. (2008) [58]. The data were processed using the ISOPLOT program (ver. 3.0) of Ludwig (2003) [59]. According to the conventional rule, the measured $^{206}Pb/^{238}U$ (<1000 Ma) and $^{207}Pb/^{206}Pb$ (>1000 Ma) ages are presented in the figures and discussions.

3.2. Zircon Lu−Hf Isotope Analysis

In situ zircon Hf isotopic analysis was carried out on a Neptune Plus MC−ICP−MS (Thermo Fisher Scientific, Bremen, Germany), coupled with a GeoLas 2005 laser-ablation system at SKLGPMR−CUG, and the detailed operating conditions and the analytical procedures were the same as described by Hu et al. (2012) [60]. We applied the directly obtained β_{Yb} value from the zircon sample itself in real time [61]. The $^{179}Hf/^{177}Hf$ and $^{173}Yb/^{171}Yb$ ratios were used to calculate the mass bias of Hf (β_{Hf}) and Yb (β_{Yb}), which were normalized to $^{179}Hf/^{177}Hf = 0.7325$ and $^{173}Yb/^{171}Yb = 1.1248$ [62] using an exponential correction for mass bias. Interference of ^{176}Yb in ^{176}Hf was corrected by measuring the interference-free ^{173}Yb isotope and using $^{176}Yb/^{173}Yb = 0.7876$ [63] to calculate $^{176}Yb/^{177}Hf$. Similarly, the relatively minor interference of ^{176}Lu in ^{176}Hf was corrected by measuring the intensity of the interference-free ^{175}Lu isotope and using the recommended $^{176}Lu/^{175}Lu = 0.02656$ [64] to calculate $^{176}Lu/^{177}Hf$. We used the mass bias of Yb (β_{Yb}) to calculate the mass fractionation of Lu because of their similar physicochemical properties. Offline selection and integration of analyte signals and mass bias calibrations were performed using ICPMSDataCal (ver. 9.0) written by Liu et al. (2010) [61].

4. Analytical Results

The results of zircon U−Pb dating are presented in Table S1 (Supplementary Materials) and the concordant diagrams (Figure 5) with corresponding relative probability plots (Figure 6). Detrital zircons with concordant U−Pb ages (concordance between 90 and 110%) were selected for in situ Hf isotopic analysis, and the results are given in Table S2 (Supplementary Materials) and plotted in Figure 7. Both a Probability Density Plot (PDP) and Kernel Density Estimation (KDE) were used to visualize the detrital age distribution patterns (Figure 6; [65]). These two methods gave similar detrital zircon peaks in Figure 6; thus, the PDP is still useful as a probability density estimator in this study. Additionally, Spencer et al. (2016) [66] documented that the discordance of zircon ages may result in a meaningless age spectrum. In Figure 5, most of the Neoproterozoic detrital zircons overlapped the 1:1 concordance line, and no negatively skewed tail in the youngest zircon population is shown in Figure 6, indicating that the effect of lead loss is negligible.

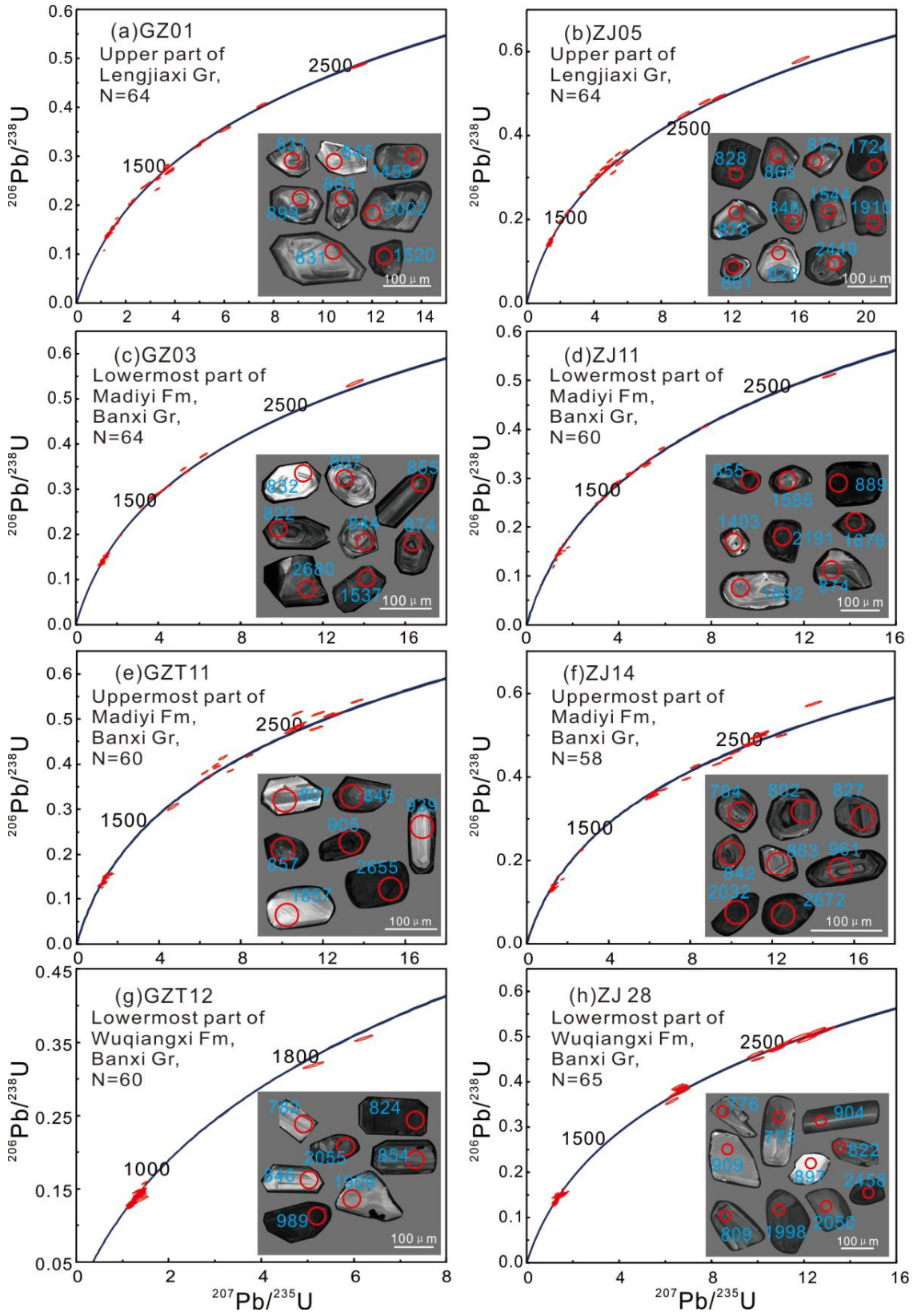


Figure 5. Zircon U–Pb concordant diagrams for studied samples. Inserted diagrams show representative CL images of analyzed zircon grains. (**a**) Sample GZ01; (**b**) sample ZJ05; (**c**) sample GZ03; (**d**) sample ZJ11; (**e**) sample GZT11; (**f**) sample ZJ14; (**g**) sample GZT12; (**h**) sample ZJ28.

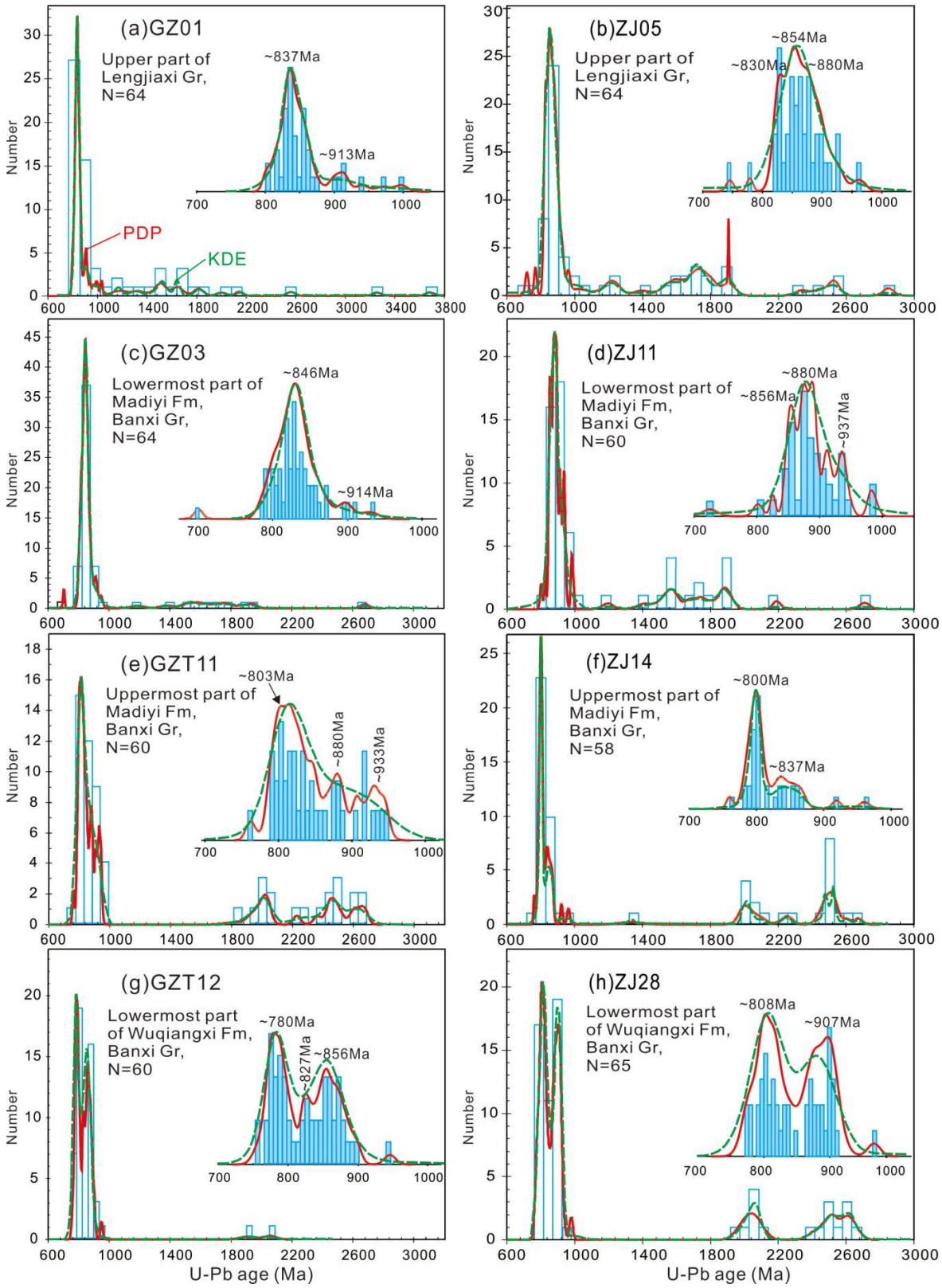


Figure 6. Relative probabilities of detrital zircons from studied samples GZ01 (**a**), ZJ05 (**b**), GZ03 (**c**), ZJ11 (**d**), GZT11 (**e**), ZJ14 (**f**), GZT12 (**g**) and ZJ28 (**h**) in Guzhang and Zhijiang areas of the WJO. PDP—Probability Density Plot; KDE—Kernel Density Estimation. $^{207}Pb/^{206}Pb$ ages are used for zircons with ages >1000 Ma, $^{206}Pb/^{238}U$ ages are used for zircons younger than 1000 Ma.

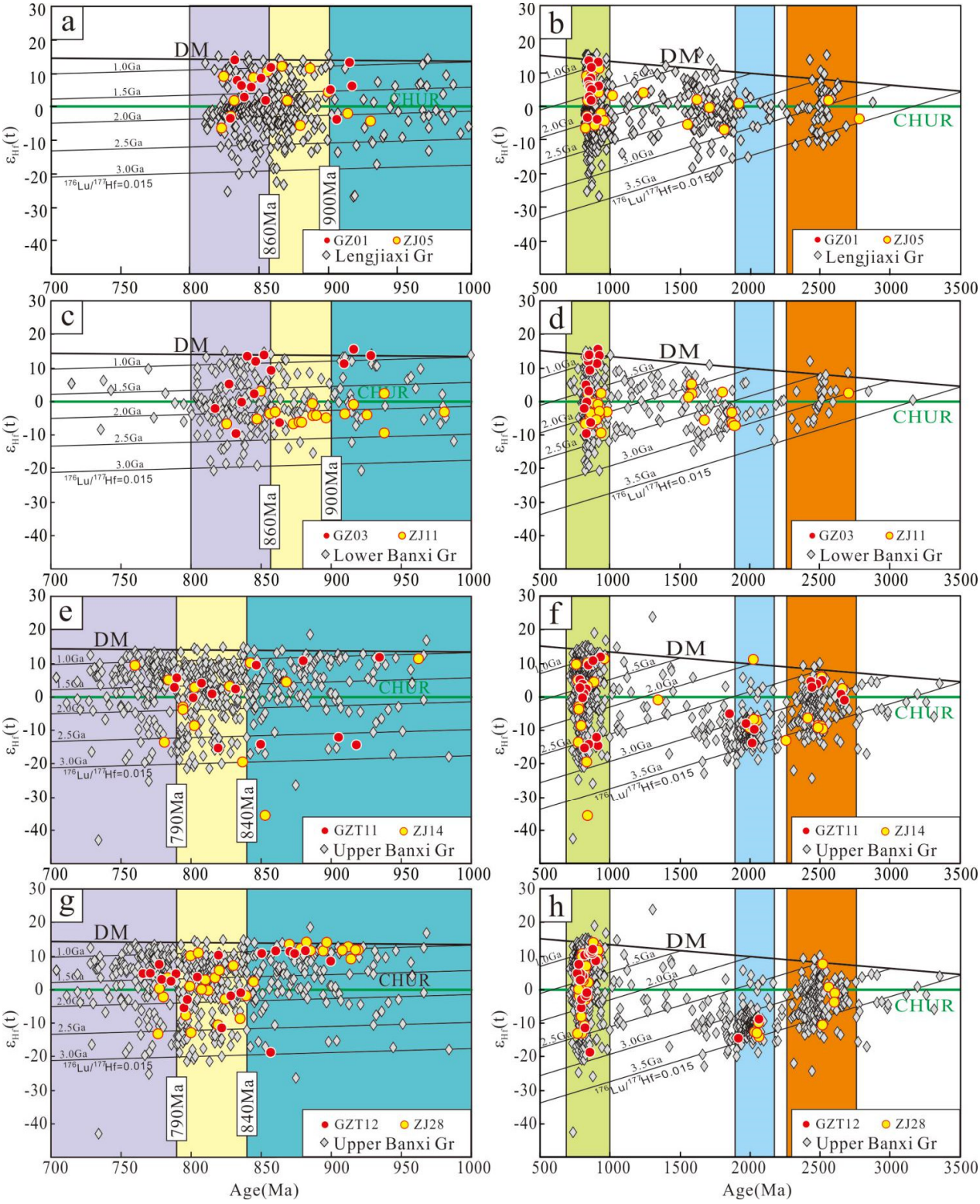


Figure 7. Plots of $\varepsilon_{Hf}(t)$ versus U–Pb ages of detrital zircons from the Lengjiaxi Group and its equivalents, upper and lower Banxi Group and their equivalents. Data sources: Lengjiaxi Group and its equivalents [18,49,67–69]; lower Banxi Group and its equivalents [18,68,70–72]; upper Banxi Group and its equivalents [44,45,68,72–76]. (**a**,**b**) Plots of $\varepsilon_{Hf}(t)$ versus U–Pb ages of samples GZ01 and ZJ05; (**c**,**d**) plots of $\varepsilon_{Hf}(t)$ versus U–Pb ages of samples GZ03 and ZJ11; (**e**,**f**) plots of $\varepsilon_{Hf}(t)$ versus U–Pb ages of samples GZT11 and ZJ14; (**g**,**h**) plots of $\varepsilon_{Hf}(t)$ versus U–Pb ages of samples GZT12 and ZJ28.

4.1. Upper Lengjiaxi Group

Sample GZ01 was collected from the upper part of the Lengjiaxi Group in Guzhang County. Sixty-five zircon grains were analyzed for U−Pb ages, although one was discarded because of discordance of more than 10% (Table S1, Supplementary Materials). Among these ages, Neoproterozoic (802−998 Ma) subhedral and oscillatory-zoned (Figure 5a) zircon grains are the dominant population and have one major age peak and a minor peak at ca. 837 Ma and ca. 913 Ma, respectively (Figure 6a). Twenty pre-Neoproterozoic zircon grains have $^{207}Pb/^{206}Pb$ ages ranging from 1.03 Ga to 3.68 Ga. The pre-Neoproterozoic zircon grains are subhedral to rounded and show partially oscillatory zoning (Figure 5a). Thirteen Neoproterozoic zircons were selected for the Hf isotopic analysis (Table S2, Supplementary Materials). Eleven Neoproterozoic (828–915 Ma) zircon grains have positive $\varepsilon_{Hf}(t)$ values (1.7 to 13.9), except for two zircon grains with negative $\varepsilon_{Hf}(t)$ values (−3.6 and −3.9) (Figure 7a).

Sample ZJ05 was collected from the upper part of the Lengjiaxi Group in Zhijiang County. Sixty-five zircon grains were analyzed for U–Pb ages, although one was discarded due to a discordance of more than 10% (Table S1, Supplementary Materials). These zircons yield a predominant age population of 822–962 Ma with two major age peaks at ca. 830 and 854 Ma (Figure 6b). Pre-Neoproterozoic zircon grains cluster at groups of 1.01–1.39 Ga, 1.54–1.91 Ga, and 2.34–2.53 Ga, and one Paleoarchean zircon grain has a $^{207}Pb/^{206}Pb$ age of 2.85 Ga. The Neoproterozoic zircon grains are subhedral and have well-preserved oscillatory zoning. The pre-Neoproterozoic zircon grains are subhedral to rounded and display partly oscillatory-zoned grains (Figure 5b). Twenty-two zircons were selected for the Hf isotopic analysis (Table S2, Supplementary Materials). The Neoproterozoic (822–928 Ma) zircon grains have variable $\varepsilon_{Hf}(t)$ values (−6.4 to 11.9) and T_{DM2} (975–1953 Ma) (Figure 7a). Two late Mesoproterozoic (1.04 and 1.23 Ga) zircon grains have relatively constant $\varepsilon_{Hf}(t)$ values of 3.6 and 4.3 and T_{DM2} of 1.57 and 1.69 Ga. Seven early Mesoproterozoic to middle Archean (1.57–2.85 Ga) zircon grains have variable $\varepsilon_{Hf}(t)$ values (−7.9 to 2.1) and T_{DM2} (2.15–3.42 Ga) (Figure 7b).

4.2. Lowermost Madiyi Formation

Sample GZ03 was collected from the lowermost part of the Madiyi Formation in Guzhang County. Sixty-five zircon grains were analyzed for U−Pb ages, although one was discarded due to a discordance of more than 10% (Table S1, Supplementary Materials). Neoproterozoic zircon grains yield an age population of 803–948 Ma, with one major age peak at ca. 846 Ma and one minor peak at ca. 914 Ma (Figure 6c). These zircons are generally euhedral to subhedral and have well preserved oscillatory zoning (Figure 5c). Pre-Neoproterozoic zircon grains are rare, with ages ranging from 1.19 Ga to 2.68 Ga. Thirteen Neoproterozoic (817−926 Ma) zircon grains were selected for the Hf isotopic analysis (Table S2, Supplementary Materials) and have variable εHf(t) values (−9.7 to 15.5) and TDM2 ages (816–2137 Ma) (Figure 7c).

Sample ZJ11 was collected from the lowermost part of the Madiyi Formation in Zhijiang County. Sixty zircon grains were analyzed for U−Pb age dating, and 27 of them were selected for the Hf isotopic analysis (Tables S1 and S2, Supplementary Materials). Among these ages, zircon grains yield two major age peaks at ca. 856 Ma and 880 Ma and three minor peaks at ca. 937 Ma, 1.59 Ga, and 1.90 Ga (Figure 6d). These zircon grains are generally subhedral to rounded with partly preserved oscillatory zoning (Figure 5d). Eighteen Neoproterozoic (825–981 Ma) zircon grains have variable $\varepsilon_{Hf}(t)$ values (−9.5 to 3.0) and T_{DM2} ages (1.4–2.21 Ga) (Figure 7c). Zircon grains with ages between 1.56 and 1.89 Ga have a wide range of $\varepsilon_{Hf}(t)$ values (−7.3 to 5.1) and T_{DM2} (1.93–2.85 Ga). One late Archean zircon grain has a positive $\varepsilon_{Hf}(t)$ value of 2.4 and an old T_{DM2} of 2.98 Ga (Figure 7d).

4.3. Uppermost Madiyi Formation

Sample GZT11 was collected from the uppermost part of the Madiyi Formation in Guzhang County. Sixty zircon grains were analyzed for U−Pb ages, and 23 of them were selected for the Hf isotopic analysis (Tables S1 and S2, Supplementary Materials). These detrital zircon grains have a predominant Neoproterozoic age group, with three age peaks at 803 Ma, 880 Ma, and 933 Ma (Figure 6e). Pre-Neoproterozoic zircon grains cluster at groups of 1.86–2.04 Ga and 2.37–2.68 Ga, with a small number of grains clustering at 2.23–2.29 Ga. These zircon grains are subhedral to rounded with partly preserved oscillatory zoning (Figure 5e). Neoproterozoic (788–934 Ma) zircon grains have variable $\varepsilon_{Hf}(t)$ values (−15.6 to 11.5) and T_{DM2} (1.06–2.48 Ga) (Figure 7e). Middle Paleoproterozoic (1.86–2.04 Ga) zircon grains have negative $\varepsilon_{Hf}(t)$ values (−14.0 to −5.3) and old T_{DM2} (2.71–3.30 Ga). Early Paleoproterozoic to late Archean (2.44–2.68 Ga) zircon grains have variable εHf(t) values (−1.2 to 4.6) and TDM2 ages (2.66–3.15 Ga) (Figure 7f).

Sample ZJ14 was obtained from the uppermost part of the Madiyi Formation in Zhijiang County. Sixty zircon grains were analyzed for U−Pb ages, although two were discarded due to a discordance of more than 10%, and 28 of them were selected for the Hf isotopic analysis (Tables S1 and S2, Supplementary Materials). The zircon grain ages are dominantly Neoproterozoic (760–961 Ma), with two age peaks at ca. 800 and 837 Ma (Figure 6f). Pre-Neoproterozoic zircon grains cluster at groups of 1.98–2.10 Ga and 2.43–2.54 Ga, with a small number of grains clustering at 2.23–2.27 Ga and 2.60–2.67 Ga. The Neoproterozoic zircon grains are generally oscillatory-zoned and subhedral. The pre-Neoproterozoic zircon grains are subhedral to rounded and partly oscillatory-zoned (Figure 5f). Neoproterozoic (760−961 Ma) zircon grains have a wide range of εHf(t) values from −35.6 to 10.6 and TDM2 from 1.05 to 3.56 Ga (Figure 7e). Five middle Paleoproterozoic (1.98–2.05 Ga) zircon grains have negative εHf(t) values (−10.2 to −6.8) and old TDM2 (2.93–3.08 Ga). Seven early Paleoproterozoic to late Archean (2.43−2.67 Ga) zircon grains have variable $\varepsilon_{Hf}(t)$ values (−9.8 to 5.5) and T_{DM2} ages (2.65−3.47 Ga) (Figure 7f).

4.4. Lowermost Wuqiangxi Formation

Detrital zircons of sample GZT12 were obtained from the lowermost part of the Wuqiangxi Formation in Guzhang County. Sixty zircon grains were analyzed for U−Pb ages, and 22 of them were selected for the Hf isotopic analysis (Tables S1 and S2, Supplementary Materials). Among these ages, Neoproterozoic zircon grains yield an age population of 757–946 Ma, with three age peaks at ca. 780, 827, and 856 Ma (Figure 6g). Pre-Neoproterozoic zircon grains are rare, with only two zircons with ages of 1.91 and 2.06 Ga. Neoproterozoic grains are generally subhedral with partly preserved oscillatory zoning. Pre-Neoproterozoic zircon grains are variably rounded (Figure 5g). Neoproterozoic (766–899 Ma) zircon grains have variable εHf(t) values (−18.7 to 11.7) and TDM2 (990–2646 Ma) (Figure 7g). Two Paleoproterozoic (1.91 and 2.06 Ga) zircon grains have negative εHf(t) values (−14.8 and −9.1) and old TDM2 (3.26 and 3.07 Ga) (Figure 7h).

Sample ZJ28 was collected from the lowermost part of the Wuqiangxi Formation in Zhijiang County. Sixty-five zircon grains were analyzed for U−Pb ages, and 40 of them were selected for the Hf isotopic analysis (Tables S1 and S2, Supplementary Materials). Among these ages, zircon grains yield a predominant Neoproterozoic (775–980 Ma) age population with two major age peaks at ca. 808 and 907 Ma (Figure 6h). Pre-Neoproterozoic zircon grains cluster at groups of 1.97–2.09 Ga and 2.40–2.65 Ga, without late Paleoproterozoic to Mesoproterozoic (1.0–1.9 Ga) zircons. Generally, most zircon grains show subhedral to rounded morphology with partly preserved oscillatory zoning (Figure 5h). Middle Neoproterozoic (775–845 Ma) zircon grains have highly variable $\varepsilon_{Hf}(t)$ values (−13.5 to 10.8) and T_{DM2} ages (991−2304 Ma). In contrast, early Neoproterozoic (870–918 Ma) zircon grains have positive $\varepsilon_{Hf}(t)$ values (9.1 to 14.0) and T_{DM2} ages ranging from 874 to 1168 Ma (Figure 7g). All Paleoproterozoic (2.03–2.07 Ga) zircon grains have negative $\varepsilon_{Hf}(t)$ values (−14.0 to −12.9) and old T_{DM2} (3.11–3.34 Ga). Late Archean (2.52–2.61 Ga) zircon grains have variable $\varepsilon_{Hf}(t)$ values (−10.5 to 7.7) and T_{DM2} (2.54–3.51 Ga) (Figure 7h).

5. Discussion

5.1. Constraints on Timing of the Middle Neoproterozoic Unconformities

5.1.1. Regional Geological Features and Timing of the Wuling Unconformity

From north to south of Hunan Province, the composition of the Madiyi Formation in the lower part of the Banxi Group changes from coarse to fine grains, the sedimentary strata become thicker, and the color of the rocks changes from purple-red to gray-green. Additionally, its contact with the underlying Lengjiaxi Group changes from a high-angular unconformity to a low-angular unconformity and disconformity, and the degree of deformation and metamorphism of the underlying Lengjiaxi Group gradually weakens in the south (Figures 8a and 9C–G; [47,48,77]). However, in northern Guangxi, sediments from the lower part of the Danzhou Group (equivalent strata of the Madiyi Formation) change from fine to coarse grains from northeast to southwest, the sedimentary strata become thinner towards the southwest, and their contact with the underlying Sibao Group changes from a disconformity to an angular unconformity (Figure 8a; [46,77]).

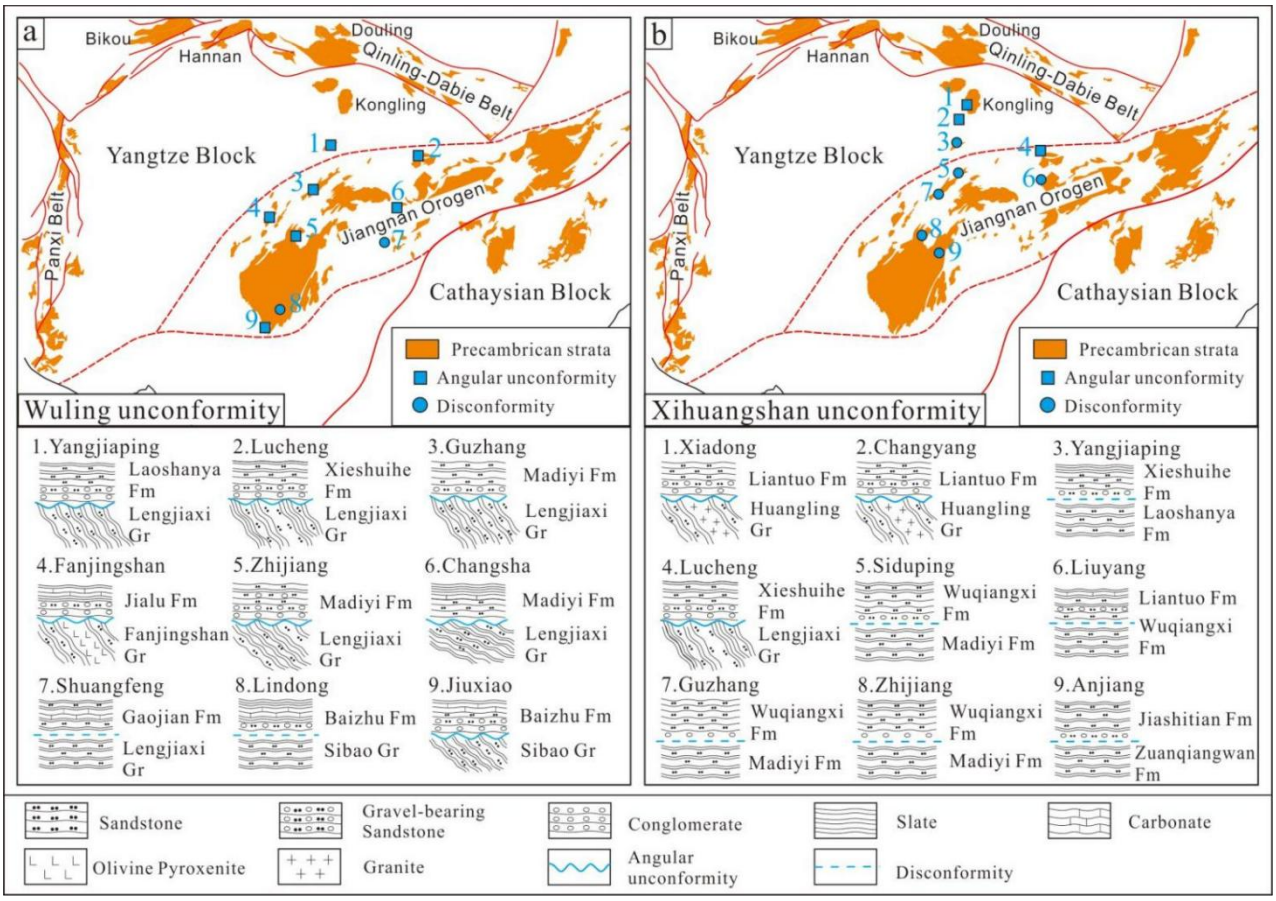


Figure 8. (**a**) Plane distribution map of Wuling unconformity (modified after [42,77]); (**b**) Plane distribution map of Xihuangshan unconformity (modified after [16,42,55,77–83]).

Dickinson and Gehrels (2009) [84] suggested that the youngest age peak is more consistent with the depositional ages of the strata than the youngest single-grain age. In this study, the youngest age peaks of detrital zircons from sandstone samples of the upper Lengjiaxi Group are ~830 Ma and ~837 Ma (Figure 6a,b; GZ01 and ZJ05), indicating that the maximum depositional age of the Lengjiaxi Group in this area is ~830 Ma. Gao et al. (2014) [85] reported a tuff at the bottom of the Banxi Group in the Zhijiang area with an age of 813.5 ± 9.6 Ma. Therefore, the timing of the Wuling unconformity in the study area could be constrained to ~830–813 Ma. Numerous studies have been conducted on the timing of the Wuling unconformity from north to south as follows. (1) The youngest detrital

zircons suggest a maximum deposition age of ~830 Ma for the Lengjiaxi Group in the Yangjiaping section, Shimen County, northwestern Hunan [41]. The tuff of the Laoshanya Formation above the Wuling unconformity was formed at 809 ± 16 Ma [83]. The timing of the Wuling unconformity was limited to ~830–809 Ma (Figure 9C). (2) The timing of the Wuling unconformity in the Lucheng section of Linxiang County in northeastern Hunan was constrained to ~822–802 Ma [86]. (3) The timing of the Wuling unconformity in Changsha, northern Hunan, has been suggested to be ~827–798 Ma [69]. (4) In the Fanjingshan region, the youngest peak age of the Fanjingshan Group below the Wuling unconformity is ~816 Ma [49], whereas the U−Pb age of the tuff above the unconformity is 814 ± 6 Ma [87], and the timing of the Wuling unconformity is limited to ~816–814 Ma. (5) The timing of the Wuling unconformity in northern Guangxi was limited to ~835–795 Ma or ~832–803 Ma (Figure 9I; [39,40]). The findings of all of the above studies are consistent with our data, thus supporting the formation of the Wuling unconformity at ~830–813 Ma in the western Jiangnan Orogen.

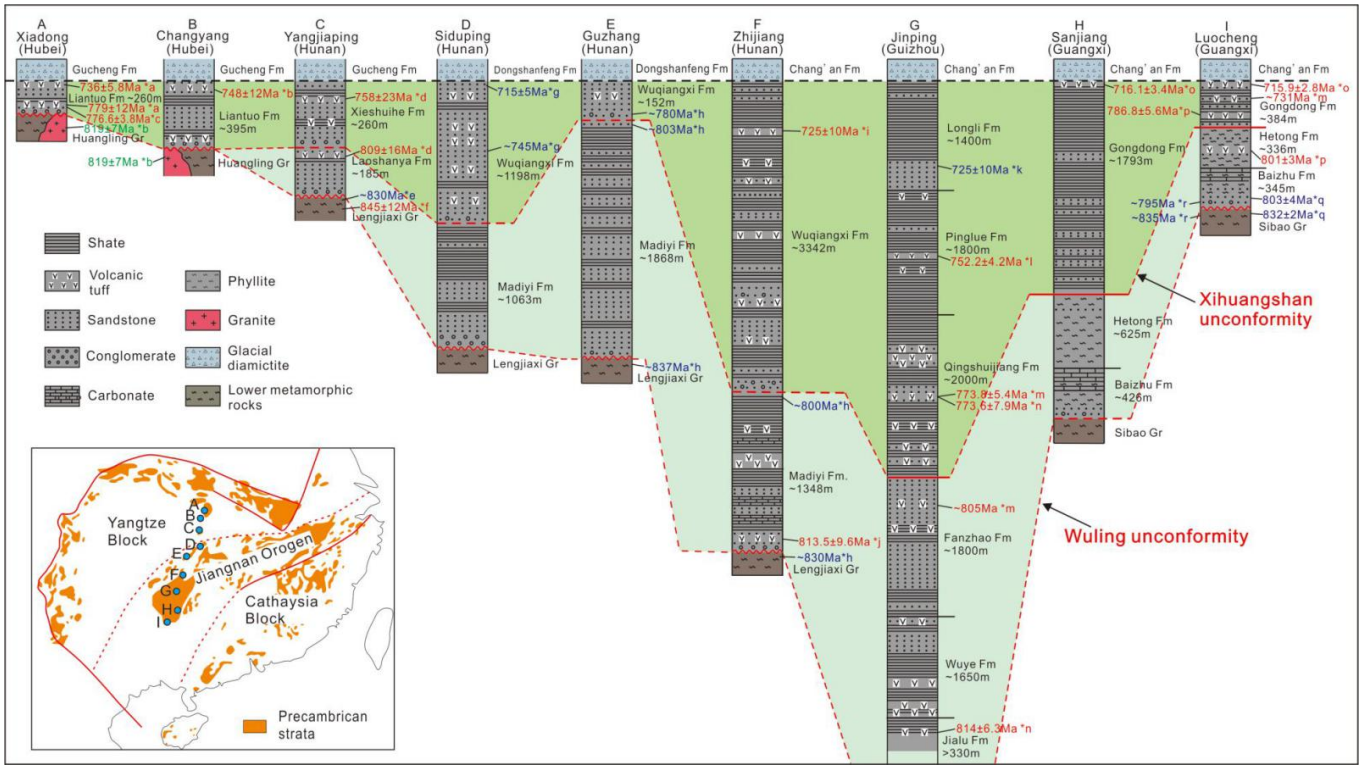


Figure 9. Stratigraphic correlation of the Neoproterozoic strata across the Yangtze Block, with most of the published U−Pb ages shown in each stratigraphic column. (**A**) Xiadong section in Hubei Province; (**B**) Changyang section in Hubei Province; (**C**) Yangjiaping section in Hunan Province; (**D**) Siduping section in Hunan Province; (**E**) Guzhang section in Hunan Province; (**F**) Zhijiang section in Hunan Province; (**G**) Jinping section in Guizhou Province; (**H**) Sanjiang section in Guangxi Province; (**I**) Luocheng section in Guangxi Province. The ages were shown in different colors according to the analyzing rock types (red: tuff/tuffaceous siltstone beds; blue: clastic rocks; green: magmatic rocks). * represents data source: (a) Du et al. [88]; (b) Ma et al. [89]; (c) Lan et al. [87]; (d) Yin et al. [83]; (e) Wang et al. [41]; (f) Sun et al. [90]; (g) Song et al. [55]; (h) this study; (i) Zhang et al. [91]; (j) Gao et al. [85]; (k) Qin et al. [52]; (l) Liu et al. [92]; (m) Wang et al. [76]; (n) Gao et al. [87]; (o) Lan et al. [93]; (p) Gao et al. [94]; (q) Su et al. [40]; (r) Ma et al. [39].

5.1.2. Regional Geological Features and Timing of the Xihuangshan Unconformity

A typical section of the Xihuangshan unconformity is located in Zhijiang County with the occurrence of bottom conglomerate and weathering crust (Figure 3f; [56]). Based on a regional comparison, it was established that the Xihuangshan unconformity is widely

distributed in Hunan Province [52,55,81], and from north to south, it changes from an angular unconformity to a disconformity and then to a conformable contact relationship (Figures 8b and 9A–I, and references therein), indicating that the Xihuangshan unconformity was formed by the uneven uplift of the block from north to south [56].

The tuff of the upper Laoshanya Formation below the Xihuangshan disconformity in the Yangjiaping section of northwestern Hunan formed at 809 ± 16 Ma [83]. Thus, the initial time of the Xihuangshan unconformity should have been later than 809 Ma. In this study, samples were collected from the top of the Madiyi Formation below the unconformity and from the bottom of the Wuqiangxi Formation above the unconformity in Guzhang and Zhijiang. The youngest detrital zircon 206Pb/238U age peaks of samples from the top of the Madiyi Formation are 803 Ma and 800 Ma (Figure 6e–f), which limits the maximum age of the Xihuangshan unconformity to ~800 Ma. In addition, the tuff age of the lower Liantuo Formation (equivalent to the Wuqiangxi Formation) in Yichang and Dahongshan areas, Hubei Province, above the Xihuangshan unconformity, are 776.6 ± 3.8 Ma and 779 ± 12 Ma, respectively [82,88]. These results are consistent with the ~780 Ma peak age of the clastic rock sample GZT12 from the bottom of the Wuqiangxi Formation (Figure 6g). Therefore, the timing of the Xihuangshan unconformity was constrained to ~800–779 Ma.

5.2. Provenance Variability of the Neoproterozoic Sedimentary Rocks

5.2.1. Provenance of the Lengjiaxi Group and the Lower Banxi Group

Based on the above study, the age groups of detrital zircon from the Lengjiaxi Group and the lower Banxi Group (and their equivalent strata) are similar, with main groupings at 800–1000 Ma, 1.50–1.90 Ga, and 2.40–2.60 Ga with one minor age population of 1.0–1.3 Ga (Figures 10 and 11, [18,23,36,39,43,52,68,70,72,74,75,95,97]), suggesting that they have identical sources.

The Neoproterozoic (800–860 Ma) detrital zircons constitute the largest and most important age group. Most zircons exhibited euhedral to subhedral morphology (Figure 5a–d), suggesting a proximal source. Many 860–760 Ma magmatic rocks are exposed in the western Jiangnan Orogen [6,7,15,22,34,95,98,99], implying that the rapid erosion of these rock assemblages may provide a potential source [40]. In this study, most of the measured zircon εHf(t) values for this age group were positive (Figure 7a,c), indicating mantle-derived magma input and juvenile crust generation. These zircons can be compared with those of ~854 Ma mafic rocks from the Yuanbaoshan area in northwest Guangxi and ~832–837 Ma granodiorite from the Dongma and Longyou areas [34,49]. Therefore, the 800–860 Ma detrital zircons mainly arose from the rapid erosion of adjacent magmatic rocks in the western Jiangnan Orogen.

The 860–1000 Ma zircons showed both positive and negative εHf(t) values (Figure 7a,c). The positive εHf(t) values of zircons correspond well to those of the magmatic rocks in the eastern Jiangnan Orogen, such as ophiolites in northeast Jiangxi Province, volcanic rocks in the Shuangxiwu arc, and ~905 Ma granitoids that intruded into the Pingshui Formation in the Shaoxing area [24,26,35,37,100]. However, 900−1000 Ma magmatic rocks with negative $\varepsilon_{Hf}(t)$ values have only been reported in the Cathaysia Block ([29] and references therein). These zircons exhibit euhedral to subhedral morphologies, suggesting relatively short transport distances. Additionally, the ~1.0–1.3 Ga, ~1.85 Ga, and ~2.50 Ga zircons are consistent with the age of the Cathaysia Block (Nanling-Yunkai region) [71,96]. Furthermore, paleocurrent analysis showed that the primary sedimentary detrital of the upper Fanjingshan Group (equivalent strata of the Lengjiaxi Group) came from the south (current coordinates) [101]. Hence, the Cathaysian Block may have been an important source of these strata. Notably, the 870–985 Ma inherited zircons reported in the 835−800 Ma S-type granite plutons in Guangxi suggest that there may be undiscovered early Neoproterozoic magmatic activity in the western Jiangnan Orogen, in which unexposed basement rocks may be the source of these sediments [40,98].

The detrital zircons of 1.5–1.90 Ga and 2.40–2.60 Ga exhibit complex morphological characteristics (Figure 5a–d), indicating that they could have diverse sources. These

age groups are similar to those from the Kunyang, Huili, Dongchuan, and Dahongshan groups [102–104] in the southwestern margin of the Yangtze Block, implying that the sediments are partly sourced from the southwestern margin of the Yangtze Block [43].

In summary, the Lengjianxi Group and lower Banxi Group (and their equivalent strata) in the western Jiangnan Orogen have similar detrital zircon age peaks, with a mixture of sources from the southwestern margin of the Yangtze Block, Cathaysia Block, and Jiangnan Orogen.

5.2.2. Provenance of the Upper Banxi Group

The detrital zircon age groups of the upper Banxi Group above the Xihuangshan unconformity mainly include 755–1000 Ma, 1.90–2.10 Ga, and 2.35–2.70 Ga, which are substantially different from those in the lower Banxi Group (Figures 10 and 11), indicating a change in provenance. Most Neoproterozoic zircons exhibited euhedral to subhedral morphologies (Figure 5g,h), suggesting proximal sources. The ratios of negative εHf(t) values of detrital zircons <840 Ma are significantly higher than those of 950–840 Ma (Figure 7e,g). This is similar to the distribution characteristics of detrital zircon εHf(t) values in the Nanhua Formation of the Yangtze Gorges area and the entire northern Yangtze Block [73], indicating that Neoproterozoic detrital zircons may have been derived from the northern part of the Yangtze Block.

Two minor age peaks of ~2.0 Ga and ~2.5 Ga in the upper Banxi Group match with those of the strata from the Kongling area in the northern Yangtze Block [42,50]. Paleoproterozoic ~2.0 Ga magmatic activities were recorded in the northern Yangtze Block, such as Kongling, Jingshan, and South Qinling [105–114]. Paleoproterozoic (1.90–2.10 Ga) zircon $\varepsilon_{Hf}(t)$ values range from −19.9 to +4.2 (Figure 7f,h), and most of them are negative (−15 to −6). This is consistent with the $\varepsilon_{Hf}(t)$ values of the Paleoproterozoic magmatic rocks from the Kongling Complex (1.80–2.20 Ga, $\varepsilon_{Hf}(t)$ = −20.6 to +4.8; [105,107,113,114]). Therefore, the detrital zircons of ~2.0 Ga may have originated from the northern Yangtze Block. The ~2.5 Ga peak age is also considered the characteristic age peak of the Yangtze Block [9,115], although the Archean magmatism of the Yangtze Block has rarely been reported. Recently, Hu et al. (2013) [116] and Wu et al. (2014) [117] reported ages of ~2.5 Ga for gneisses from the Douling Complex, proving the existence of early Paleoproterozoic to late Archean basement rocks in the northern Yangtze Block. Furthermore, the 2.65–2.75 Ga magmatism is widespread in the northern margin of the Yangtze Block, such as ~2.70–2.60 Ga A-type granitic gneisses [118], ~2.66 Ga biotite granites, and ~2.70–2.64 Ga two-mica granites [119] in the Kongling terrane, with ~2.65 Ga A-type granites in the Huji area [120,121]. Thus, the detrital zircons of ~2.5 Ga and 2.65–2.75 Ga may also come from the northern Yangtze Block. Additionally, as shown in Figure 10, the ratio of ~2.0 Ga and ~2.5 Ga detrital zircons is larger near the northern margin of the Yangtze Block and gradually decreases or disappears toward the south, implying that the detrital zircons of ~2.0 Ga and ~2.5 Ga spread southward from the northern margin of the Yangtze Block. Notably, detrital zircons of ~2.0 Ga and ~2.5 Ga in the upper Danzhou Group (equivalent to Wuqiangxi Formation) in northern Guangxi have disappeared (Figure 10G), indicating that no clastic sediment was received from the northern margin of the Yangtze Block. Therefore, we suggest that the provenance of the Upper Danzhou Group was derived mainly from the Jiangnan Orogen.

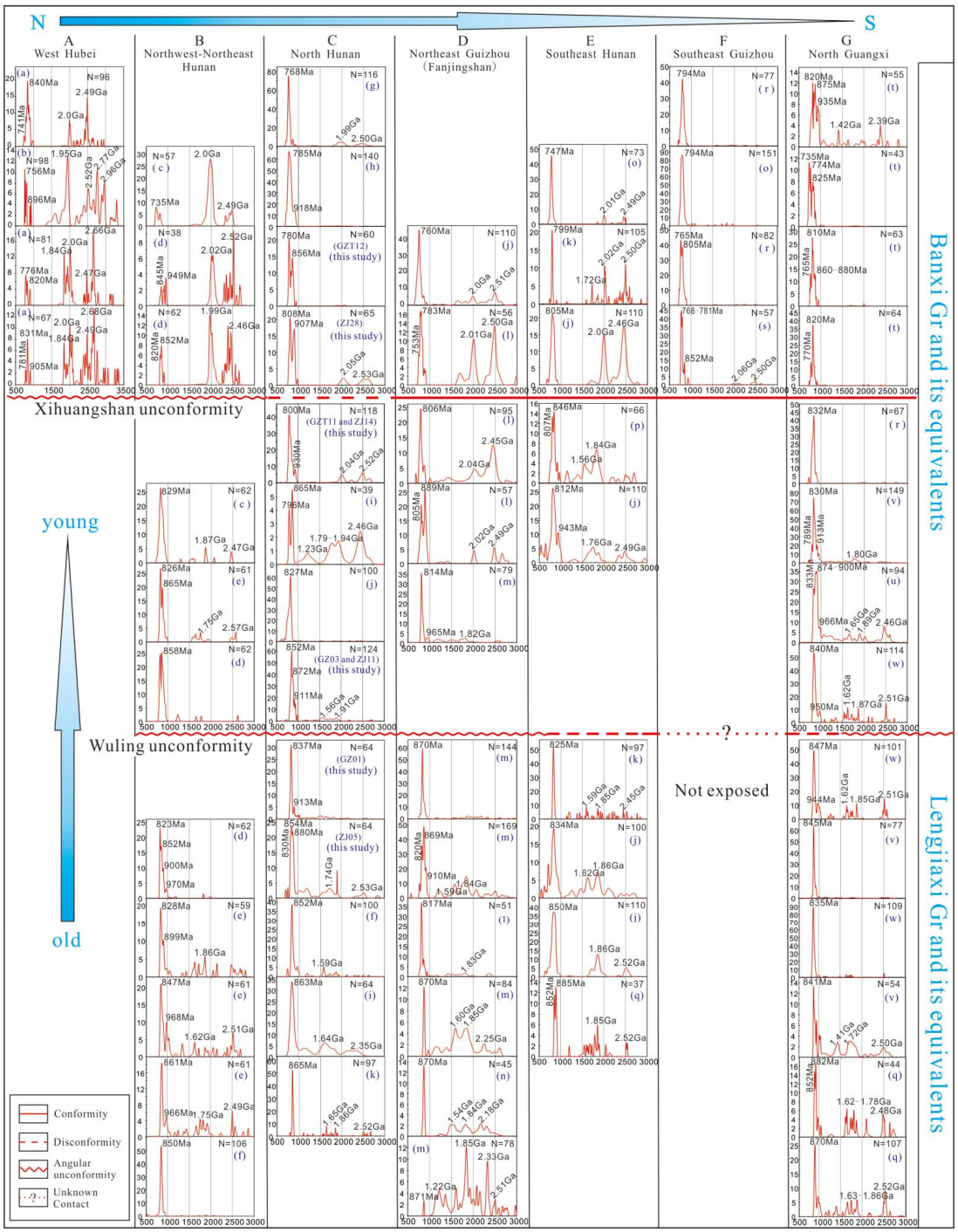


Figure 10. U−Pb age histograms of the detrital zircons from Banxi and Lengjiaxi groups and their equivalents in the west Hubei (**A**), northwest–northeast Hunan (**B**), north Hunan (**C**), northeast Guizhou (**D**), southeast Hunan (**E**), southeast Guizhou (**F**) and north Guangxi (**G**) from the Yangtze Block. Lowercase letters in parentheses represent data sources: (**a**) Liu et al. [73]; (**b**) Zhang et al. [122]; (**c**) Yan et al. [72]; (**d**) Wang et al. [75]; (**e**) Wang et al. [69]; (**f**) Zhang et al. [36]; (**g**) Liu et al. [123]; (**h**) Song et al. [55]; (**i**) Zhang et al. [97]; (**j**) Su et al. [96]; (**k**) Meng et al. [68]; (**l**) Wang et al. [74]; (**m**) Zhang et al. [43]; (**n**) Zhou et al. [95]; (**o**) Wang et al. [76]; (**p**) Wang et al. [70]; (**q**) Wang et al. [23]; (**r**) Qin et al. [52]; (**s**) Wei et al. [124]; (**t**) Wang and Zhou, [44]; (**u**) Wang et al. [71]; (**v**) Ma et al. [39]; (**w**) Yang et al. [18]; and this study. $^{207}Pb/^{206}Pb$ ages are used for zircons with ages >1000 Ma, $^{206}Pb/^{238}U$ ages are used for zircons younger than 1000 Ma.

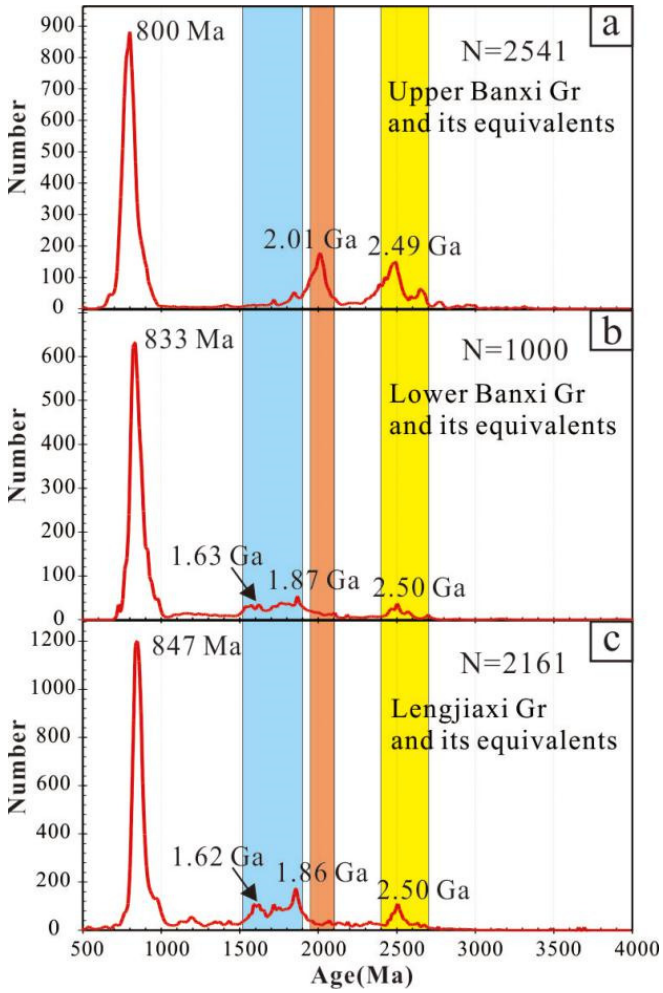


Figure 11. A comparison of age probability histograms of representative zircon age distributions for the lower Banxi Group and its equivalents (**a**), the upper Banxi Group and its equivalents (**b**), and the Lengjiaxi Group and its equivalents (**c**) along the WJO, respectively. Data from: [18,23,36,39,43,44,52,55,68–76,95–97,122–124] and this study. $^{207}Pb/^{206}Pb$ ages are used for zircons with ages >1000 Ma, $^{206}Pb/^{238}U$ ages are used for zircons younger than 1000 Ma.

In conclusion, the provenance of the upper and lower parts of the Banxi Group in the western Jiangnan Orogen changed above the Xihuangshan unconformity, and the provenance of the upper Banxi Group mainly came from the northern Yangtze Block and partly from the Jiangnan Orogen.

5.3. Implications for the Tectonic Evolution

As mentioned above, the Lengjianxi Group below the Wuling unconformity and lower Banxi Group above the Wuling unconformity have similar detrital zircon age spectra, indicating that the provenance did not change across this unconformity. Provenance analysis suggests that these strata have received materials from the Cathaysia Block, implying that the Yangtze Block and the Cathaysia Block probably collided in the western Jiangnan Orogen earlier than the formation of the upper Lengjixi Group and earlier than the timing of the Wuling unconformity. In the eastern Jiangnan Orogen, the Fuchuan continental margin arc in southern Anhui may have lasted until 820 Ma, and the Fuchuan ophiolite (FCO complex) of 840–824 Ma represents the final amalgamation between the Yangtze and Cathaysia [125]. In addition, the ~820 Ma cordierite-bearing granodiorites are characterized by high ASI values (peraluminous), positive $\varepsilon_{Hf}(t)$ values, and high $\delta^{18}O$ values and record the arc–continent collision orogeny in southern Anhui [126]. The ~800 Ma composite dikes

intruded into these S-type granitoids, indicating that postorogenic extension occurred shortly after the Neoproterozoic orogeny [127]. Thus, arc–continent collision in the eastern Jiangnan Orogen may have occurred mainly during the period 820–800 Ma [128]. Therefore, the Yangtze and Cathaysia blocks collided earlier in the western Jiangnan Orogen than in the eastern Jiangnan Orogen, exhibiting a scissor-like closure process (Figure 12a).

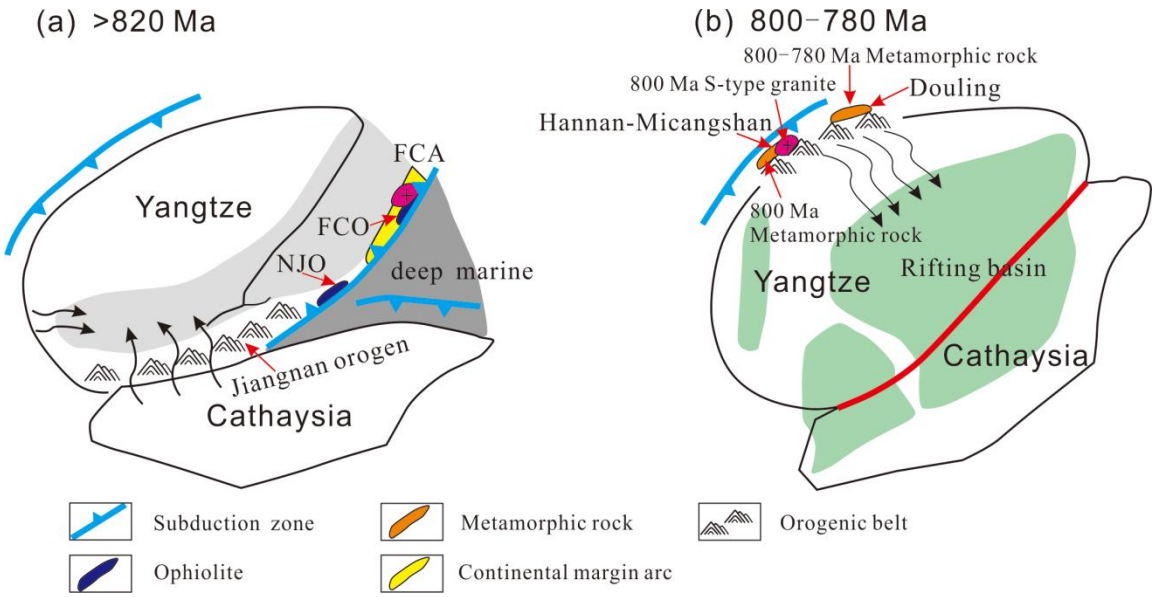


Figure 12. Scheme illustrating the orogenic events around the Yangtze Block. (**a**) A scissor-like closure process occurred in the southeastern margin of the Yangtze Block; (**b**) 800–780 Ma collisional orogeny in the northern and northwestern margins of the Yangtze Block (NJO—Northern Jiangxi ophiolite; FCO—840–820 Ma SSZ-type Fuchuan ophiolite; FCA—Fuchuan continental margin arc; Modified after [17,125]).

In this study, the timing of the Xihuangshan unconformity was constrained to ~800–779 Ma. The contact relationship of the Xihuangshan unconformity transitioned from an angular unconformity to a disconformity and conformity from north to south (Figure 8b and references therein), indicating that the Xihuangshan unconformity spread from north to south. Additionally, a change in provenance occurred between the upper and lower Banxi groups. The detrital zircons in the lower Banxi Group were mainly derived from the southwestern margin of the Yangtze Block, Cathaysia Block, and Jiangnan Orogen, whereas the detrital zircons in the upper Banxi Group mainly came from the northern margin of the Yangtze Block. Moreover, the proportion of ~2.0 Ga and ~2.5 Ga detrital zircons is larger near the northern margin of the Yangtze Block and gradually decreases or even disappears to the south, indicating that the transmission path is from the north to south (Figure 10). Therefore, we propose that the main driver of the Xihuangshan unconformity comes from the northern margin of the Yangtze Block.

Previous studies have reported abundant Neoproterozoic magmatism and long-term subduction (870–740 Ma) at the northwestern and northern margins of the Yangtze Block [51,129]. Based on the changes in $\varepsilon_{Hf}(t)$ values, Yang et al. (2018) [42] suggested that a collision may have occurred in the northern Yangtze Block at ~790 Ma. In the Dahongshan area, northern Yangtze Block, the Liantuo Formation overlies the Huashan Group with an angular unconformity formed at 810–780 Ma [42,130,131], which may have been caused by collision orogeny. Moreover, 800–780 Ma high amphibolite facies metamorphism has been reported in South Qinling, representing the collision between the Douling Block and the Yangtze Block [115,132]. The contemporary ~800 Ma upper amphibolite to granulite-facies metamorphism and peraluminous granite in the northwestern part of the Yangzte Block [133,134] were proposed to have been generated at the syncollision stage (Figure 12b).

These studies indicate a collisional orogeny of ~800–780 Ma in the northern and northwestern margins of the Yangtze Block. It is suggested that the Xihuangshan unconformity may be induced by collisional events in the northern and northwestern margins of the Yangtze Block, combined with provenance transition and unconformity distribution characteristics.

6. Conclusions

The formation time of the Wuling unconformity is ~830–813 Ma, whereas that of the Xihuangshan unconformity is ~800–779 Ma;

Provenance analysis shows that the upper Lengjiaxi Group and lower Banxi Group in the research areas have similar detrital zircon age spectra with age groups of 800–1000 Ma, 1.50–1.90 Ga, and 2.40–2.60 Ga, indicating that the provenance has not changed. The detrital zircon U−Pb chronology and Hf isotope characteristics suggest that the sediments were sourced from the southwestern margin of the Yangtze Block, Cathaysia Block, and Jiangnan Orogen. The appearance of the provenance of the Cathaysia Block in the upper Lengjiaxi Group implies that the collision of the Yangtze Block and Cathaysia Block in the western Jiangnan Orogen occurred much earlier than the Wuling unconformity (~830–813 Ma) and earlier than that in the eastern Jiangnan Orogen. Thus, the collision between the Yangtze and Cathaysia blocks may have undergone a scissor-like closure process from west to east;

Above the Xihuangshan unconformity, the provenance of the sedimentary strata changed. The contact relationship and provenance transition demonstrate that the Xihuangshan unconformity is a tectonic unconformity spreading from north to south, coeval with the collision orogeny in the northern and northwestern margins of the Yangtze Block at approximately 800–780 Ma. This unconformity may have been driven by a collision orogeny in the northern and northwestern margins of the Yangtze Block.

Supplementary Materials: The following are available online at https://www.mdpi.com/article/10.3390/min12050596/s1, Table S1: LA-ICP-MS zircon U–Th–Pb isotope analyses for detrital zircons from Neoproterozoic sedimentary rocks in the western Jiangnan Orogen, South China, Table S2: LA-MC-ICP-MS Hf isotope compositions of detrital zircons from Neoproterozoic sedimentary rocks in the western Jiangnan Orogen, South China.

Author Contributions: Conceptualization, D.L. and Z.Y.; methodology, Y.L.; software, D.L. and D.W.; validation, D.L. and Z.Y.; formal analysis, K.Y.; investigation, D.L. and Y.L.; data curation, D.W. and P.C.; writing—original draft preparation, D.L. and P.C.; writing—review and editing, Z.Y. and D.L.; supervision, K.Y.; funding acquisition, Z.Y. and K.Y. All authors have read and agreed to the published version of the manuscript.

Funding: This study was supported by the Hebei Natural Science Foundation (Grant No. D2020403095), the National Natural Science Foundation of China (Grant Nos. 41172189 and 41472190), the Youth Science and Technology Foundation of Hebei GEO University (Grant No. QN202125), the Ph.D. Research Startup Foundation of Hebei GEO University (Grant No. BQ2018011).

Data Availability Statement: Data are contained within the supplementary materials.

Acknowledgments: We greatly appreciate the help of Siming Lu during daily discussion work and the editor and reviewers for their suggestions and corrections to improve the paper.

Conflicts of Interest: The authors declare no conflict of interest.

References

1. Condie, K.C. Continental Growth during Formation of Rodinia at 1.35–0.9 Ga. *Gondwana Res.* **2001**, *4*, 5–16. [CrossRef]
2. Li, Z.X.; Bogdanova, S.V.; Collins, A.S.; Davidson, A.; De Waele, B.; Ernst, R.E.; Fitzsimons, I.C.W.; Fuck, R.A.; Gladkochub, D.P.; Jacobs, J.; et al. Assembly, Configuration, and Break-up History of Rodinia: A Synthesis. *Precambrian Res.* **2008**, *160*, 179–210. [CrossRef]
3. Evans, D.A. The Palaeomagnetically Viable, Long-Lived and All-Inclusive Rodinia Supercontinent Recon-Struction. *Geol. Soc. Lond. Spec. Publ.* **2009**, *327*, 371–404. [CrossRef]
4. Li, Z.X.; Zhang, L.; Powell, C.M. South China in Rodinia: Part of the Missing Link between Australia–East Antarctica and Laurentia? *Geology* **1995**, *23*, 407–410. [CrossRef]

5. Dong, Y.P.; Liu, X.M.; Santosh, M.; Zhang, X.N.; Chen, Q.; Yang, C.; Yang, Z. Neoproterozoic Subduction Tectonics of the Northwestern Yangtze Block in South China: Constrains from Zircon U-Pb Geochronology and Geochemistry of Mafic Intrusions in the Hannan Massif. *Precambrian Res.* **2011**, *189*, 66–90. [CrossRef]
6. Li, X.H. U–Pb Zircon Ages of Granites from the Southern Margin of the Yangtze Block: Timing of Neoprote-Rozoic Jinning Orogeny in SE China and Implications for Rodinia Assembly. *Precambrian Res.* **1999**, *97*, 43–57. [CrossRef]
7. Li, Z.X.; Li, X.H.; Kinny, P.D.; Wang, J. The Breakup of Rodinia: Did It Start with a Mantle Plume beneath South China? *Earth Planet. Sci. Lett.* **1999**, *173*, 171–181. [CrossRef]
8. Shu, L.S.; Faure, M.; Yu, J.H.; Jahn, B.M. Geochronological and Geochemical Features of the Cathaysia Block (South China): New Evidence for the Neoproterozoic Breakup of Rodinia. *Precambrian Res.* **2011**, *187*, 263–276. [CrossRef]
9. Li, X.H.; Li, W.X.; He, B. Building of the South China Block and Its Relevance to Assembly and Breakup of Rodinia Supercontinent: Observations, Interpretations and Tests. *Bull. Mineral. Petrol. Geochem.* **2012**, *31*, 543–559. (In Chinese with English abstract)
10. Zhao, G.C.; Cawood, P.A. Precambrian Geology of China. *Precambrian Res.* **2012**, *222–223*, 13–54. [CrossRef]
11. Cawood, P.A.; Strachan, R.A.; Pisarevsky, S.A.; Gladkochub, D.P.; Murphy, J.B. Linking Collisional and Accretionary Orogens during Rodinia Assembly and Breakup: Implications for Models of Supercontinent Cycles. *Earth Planet. Sci. Lett.* **2016**, *449*, 118–126. [CrossRef]
12. Yu, J.H.; O'Reilly, S.Y.; Wang, L.J.; Griffin, W.L.; Zhang, M.; Wang, R.C.; Jiang, S.Y.; Shu, L.S. Where was South China in the Rodinia Supercontinent? Evidence from U-Pb Geochronology and Hf Isotopes of Detrital Zircons. *Precambrian Res.* **2008**, *164*, 1–15. [CrossRef]
13. Zheng, Y.F.; Wu, R.X.; Wu, Y.B.; Zhang, S.B.; Yuan, H.; Wu, F.Y. Rift Melting of Juvenile Arc-Derived Crust: Geochemical Evidence from Neoproterozoic Volcanic and Granitic Rocks in the Jiangnan Orogen, South China. *Precambrian Res.* **2008**, *163*, 351–383. [CrossRef]
14. Zheng, Y.F.; Xiao, W.J.; Zhao, G. Introduction to Tectonics of China. *Gondwana Res.* **2013**, *23*, 1189–1206. [CrossRef]
15. Li, X.H.; Li, Z.X.; Ge, W.C.; Zhou, H.W.; Li, W.X.; Liu, Y.; Wingate, M.T.D. Neoproterozoic Granitoids in South China: Crustal Melting above a Mantle Plume at ca 825 Ma? *Precambrian Res.* **2003**, *122*, 45–83. [CrossRef]
16. Wang, J.; Li, Z.X. History of Neoproterozoic Rift Basins in South China: Implications for Rodinia Break-up. *Precambrian Res.* **2003**, *122*, 141–158. [CrossRef]
17. Zhang, C.L.; Li, H.K.; Santosh, M. Revisiting the Tectonic Evolution of South China: Interaction between the Rodinia Superplume and Plate Subduction? *Terra Nova* **2013**, *25*, 212–220. [CrossRef]
18. Yang, C.; Li, X.H.; Wang, X.C.; Lan, Z. Mid-Neoproterozoic Angular Unconformity in the Yangtze Block Revisited: Insights from Detrital Zircon U-Pb Age and Hf–O Isotopes. *Precambrian Res.* **2015**, *266*, 165–178. [CrossRef]
19. Zhou, M.F.; Yan, D.P.; Kennedy, A.K.; Li, Y.; Ding, J. SHRIMP U–Pb Zircon Geochronological and Geochemical Evidence for Neoproterozoic Arc-Magmatism along the Western Margin of the Yangtze Block, South China. *Earth Planet Sci. Lett.* **2002**, *196*, 51–67. [CrossRef]
20. Zhao, J.H.; Zhou, M.F. Geochemistry of Neoproterozoic Mafic Intrusions in the Panzhihua District (Sichuan Province, SW China): Implications for Subduction-Related Metasomatism in the Upper Mantle. *Precambrian Res.* **2007**, *152*, 27–47. [CrossRef]
21. Zhao, J.H.; Zhou, M.F.; Yan, D.P.; Zeng, J.P.; Li, J.W. Reappraisal of the Ages of Neoproterozoic Strata in South China: No Connection with the Grenvillian Orogeny. *Geology* **2011**, *39*, 299–302. [CrossRef]
22. Zheng, Y.F.; Zhang, S.B.; Zhao, Z.F.; Wu, Y.B.; Li, X.; Li, Z.; Wu, F.Y. Contrasting Zircon Hf and O Isotopes in the Two Episodes of Neoproterozoic Granitoids in South China: Implications for Growth and Reworking of Continental Crust. *Lithos* **2007**, *96*, 127–150. [CrossRef]
23. Wang, X.L.; Zhou, J.C.; Griffin, W.L.; Wang, R.C.; Qiu, J.S.; O'Reilly, S.Y.; Xu, X.; Liu, X.M.; Zhang, G.L. Detrital Zircon Geochronology of Precambrian Basement Sequences in the Jiangnan Orogen: Dating the Assembly of the Yangtze and Cathaysia Blocks. *Precambrian Res.* **2007**, *159*, 117–131. [CrossRef]
24. Ye, M.F.; Li, X.H.; Li, W.X.; Liu, Y.; Li, Z.X. SHRIMP zircon U–Pb Geochronological and Whole-Rock Geochemical Evidence for an Early Neoproterozoic Sibaoan Magmatic Arc along the Southeastern Margin of the Yangtze Block. *Gondwana Res.* **2007**, *12*, 144–156. [CrossRef]
25. Li, W.X.; Li, X.H.; Li, Z.X.; Lou, F.S. Obduction-Type Granites within the NE Jiangxi Ophiolite: Implications for the Final Amalgamation between the Yangtze and Cathaysia Blocks. *Gondwana Res.* **2008**, *13*, 288–301. [CrossRef]
26. Li, X.H.; Li, W.X.; Li, Z.X.; Lo, C.H.; Wang, J.; Ye, M.F.; Yang, Y.H. Amalgamation between the Yangtze and Cathaysia Blocks in South China: Constraints from SHRIMP U–Pb Zircon Ages, Geochemistry and Nd–Hf Isotopes of the Shuangxiwu Volcanic Rocks. *Precambrian Res.* **2009**, *174*, 117–128. [CrossRef]
27. Shu, L.S. An Analysis of Principal Features of Tectonic Evolution in South China Block. *Geol. Bull. China* **2012**, *31*, 1035–1053, (In Chinese with English abstract).
28. Shu, L.S.; Yao, J.L.; Wang, B.; Faure, M.; Charvet, J.; Chen, Y. Neoproterozoic Plate Tectonic Process and Phanerozoic Geodynamic Evolution of the South China Block. *Earth-Sci. Rev.* **2021**, *216*, 103596. [CrossRef]
29. Xia, Y.; Xu, X.S.; Niu, Y.L.; Liu, L. Neoproterozoic Amalgamation between Yangtze and Cathaysia Blocks: The Magmatism in Various Tectonic Settings and Continent-Arccontinent Collision. *Precambrian Res.* **2018**, *309*, 56–87. [CrossRef]
30. Yao, J.L.; Cawood, P.A.; Shu, L.S.; Santosh, M.; Li, J.Y. An Early Neoproterozoic Accretionary Prism Ophiolitic Melange from the Western Jiangnan Orogenic Belt, South China. *J. Geol.* **2016**, *124*, 587–601. [CrossRef]

31. Yao, J.L.; Cawood, P.A.; Shu, L.S.; Zhao, G.C. Jiangnan Orogen, South China: A ~970–820 Ma Rodinia Margin Accretionary Belt. *Earth-Sci. Rev.* **2019**, *196*, 102872. [CrossRef]
32. Zhou, J.C.; Wang, X.L.; Qiu, J.S.; Gao, J. Geochemistry of Meso- and Neoproterozoic Mafic-Ultramafic Rocks from Northern Guangxi, China: Arc or Plume Magmatism? *Geochem. J.* **2004**, *38*, 139–152. [CrossRef]
33. Zhang, K.J. A Mediterranean-Style Model for Early Neoproterozoic Amalgamation of South China. *J. Geodyn.* **2017**, *105*, 1–10. [CrossRef]
34. Yao, J.L.; Shu, L.S.; Santosh, M.; Zhao, G.C. Neoproterozoic Arc-Related Mafic-Ultramafic Rocks and Syn-Collision Granite from the Western Segment of the Jiangnan Orogen, South China: Constraints on the Neoproterozoic Assembly of the Yangtze and Cathaysia Blocks. *Precambrian Res.* **2014**, *243*, 39–62. [CrossRef]
35. Zhang, C.L.; Zou, H.B.; Zhu, Q.B.; Chen, X.Y. Late Mesoproterozoic to Early Neoproterozoic Ridge Subduction along Southern Margin of the Jiangnan Orogen: New Evidence from the Northeastern Jiangxi Ophiolite (NJO), South China. *Precambrian Res.* **2015**, *268*, 1–15. [CrossRef]
36. Zhang, H.; Li, T.; Xie, Y.; Zhang, C.; Gao, L.; Geng, S.; Chen, T.; You, G. Geochronology and Tectonic Evolution of the West Section of the Jiangnan Orogenic Belt. *Acta Geol. Sin.-Engl. Ed.* **2015**, *89*, 1497–1515.
37. Wang, X.S.; Gao, J.; Klemd, R.; Jiang, T.; Zhai, Q.G.; Xiao, X.C.; Liang, X.Q. Early Neoproterozoic Multiple Arc–Back-Arc System Formation during Subduction–Accretion Processes between the Yangtze and Cathaysia Blocks: New Constraints from the Supra-Subduction Zone NE Jiangxi Ophiolite (South China). *Lithos* **2015**, *236–237*, 90–105. [CrossRef]
38. Zhao, G.C. Jiangnan Orogen in South China: Developing from Divergent Double Subduction. *Gondwana Res.* **2015**, *27*, 1173–1180. [CrossRef]
39. Ma, X.; Yang, K.G.; Li, X.G.; Dai, C.G.; Zhang, H.; Zhou, Q. Neoproterozoic Jiangnan Orogeny in Southeast Guizhou, South China: Evidence from U-Pb ages for Detrital Zircons from the Sibao Group and Xiajiang Group. *Can. J. Earth Sci.* **2016**, *53*, 219–230. [CrossRef]
40. Su, H.M.; Jiang, S.Y.; Mao, J.; Zhang, D.; Wu, X.; Qin, H. U-Pb Ages and Lu-Hf Isotopes of Detrital Zircons from Sedimentary Units across the Mid-Neoproterozoic Uncon-Formity in the Western Jiangnan Orogen of South China and Their Tectonic Implications. *J. Geol.* **2018**, *126*, 207–228. [CrossRef]
41. Wang, W.; Wang, F.; Chen, F.; Zhu, X.; Xiao, P.; Siebel, W. Detrital Zircon Ages and Hf-Nd Isotopic Composition of Neoproterozoic Sedimentary Rocks in the Yangtze Block: Constraints on the Deposition Age and Provenance. *J. Geol.* **2010**, *118*, 79–94. [CrossRef]
42. Yang, Z.N.; Yang, K.G.; Polat, A.; Xu, Y. Early Crustal Evolution of the Eastern Yangtze Block: Evidence from Detrital Zircon U-Pb Ages and Hf Isotopic Composition of the Neoproterozoic Huashan Group in the Dahongshan Area. *Precambrian Res.* **2018**, *309*, 248–270. [CrossRef]
43. Zhang, J.W.; Ye, T.P.; Dai, Y.; Chen, J.; Zhang, H.; Dai, C.G.; Yuan, G.; Jiang, K. Provenance and Tectonic Setting Transition as Recorded in the Neoproterozoic Strata, Western Jiangnan Orogen: Implications for South China within Rodinia. *Geosci. Front.* **2019**, *10*, 1823–1839. [CrossRef]
44. Wang, W.; Zhou, M.F. Sedimentary Records of the Yangtze Block (South China) And Their Correlation with Equivalent Neoproterozoic Sequences on Adjacent Continents. *Sed. Geol.* **2012**, *265–266*, 126–142. [CrossRef]
45. Wang, L.J.; Griffin, W.L.; Yu, J.H.; O'Reilly, S.Y. U-Pb and Lu–Hf Isotopes in Detrital Zircon from Neoproterozoic Sedimentary Rocks in the Northern Yangtze Block: Implications for Precambrian Crustal Evolution. *Gondwana Res.* **2013**, *23*, 1261–1272. [CrossRef]
46. BGMRGX. *Regional Geology of Guangxi Province*; Geological Publishing House: Beijing, China, 1985. (In Chinese with English abstract)
47. BGMRGZ. *Regional Geology of Guizhou Province*; Geological Publishing House: Beijing, China, 1987. (In Chinese with English abstract)
48. BGMRHN. *Regional Geology of Hunan Province*; Geological Publishing House: Beijing, China, 1988. (In Chinese with English abstract)
49. Wang, X.L.; Zhou, J.C.; Griffin, W.L.; Zhao, G.; Yu, J.H.; Qiu, J.S.; Zhang, Y.J.; Xing, G.F. Geochemical Zonation across a Neoproterozoic Orogenic Belt: Isotopic Evidence from Granitoids and Metasedimentary Rocks of the Jiangnan Orogen, China. *Precambrian Res.* **2014**, *242*, 154–171. [CrossRef]
50. Sun, J.J.; Shu, L.S.; Santosh, M.; Wang, L.S. Precambrian Crustal Evolution of the Central Jiangnan Orogenic Belt (South China): Evidence from Detrital Zircon U-Pb Ages and Hf Isotopic Compositions of Neoproterozoic Metasedimentary Rocks. *Precambrian Res.* **2018**, *318*, 1–24. [CrossRef]
51. Zhao, J.H.; Li, Q.W.; Liu, H.; Wang, W. Neoproterozoic Magmatism in the Western and Northern Margins of the Yangtze Block (South China) Controlled by Slab Subduction and Subduction-Transform-Edge-Propagator. *Earth-Sci. Rev.* **2018**, *187*, 1–18. [CrossRef]
52. Qin, Y.J.; Du, Y.S.; Mou, J.; Lu, D.B.; Long, J.X.; Wang, A.H.; Zhang, H.S.; Zeng, C.X. Geochronology of Neoproterozoic Xiajiang Group in Southeast Guizhou, South China, and Its Geological Implications. *Earth Sci.-J. China Univ. Geosci.* **2015**, *40*, 1107–1120, (In Chinese with English abstract).
53. Cui, X.Z.; Jiang, X.S.; Deng, Q.; Wang, J.; Zhuo, J.W.; Ren, G.; Cai, J.; Wu, H.; Jiang, Z. Zircon U-Pb Geochronological Results of the Danzhou Group in Northern Guangxi and Their Implications for the Neoproterozoic Rifting Stages in South China. *Geotecton. Metallog.* **2016**, *40*, 1049–1063. (In Chinese with English abstract)
54. Zhou, C.M. Neoproterozoic Lithostratigraphy and Correlation across the Yangtze Block, South China. *J. Stratigr.* **2016**, *40*, 120–135. (In Chinese with English abstract)

55. Song, G.Y.; Wang, X.Q.; Shi, X.Y.; Jiang, G.Q. New U-Pb Age Constraints on the Upper Banxi Group and Synchrony of the Sturtian Glaciation in South China. *Geosci. Front.* **2017**, *8*, 1161–1173. [CrossRef]
56. BGMRHN. *Stratigraphy (Lithostratic) of Hunan Province*; China University of Geosciences Press: Wuhan, China, 1997; p. 292. (In Chinese)
57. Luo, L.; Sun, H.Q.; Huang, J.Z.; Zhang, X.Y. Sedimentary Environment Analysis and Regional Comparison of Wuqiangxi Formation in Northwestern Hunan Province. *Geol. Miner. Resour. South China* **2013**, *29*, 183–191. (In Chinese with English abstract)
58. Liu, Y.S.; Hu, Z.C.; Gao, S.; Günther, D.; Xu, J.; Gao, C.G.; Chen, H.H. In Situ Analysis of Major and Trace Elements of Anhydrous Minerals by LA-ICP-MS without Applying an Internal Standard. *Chem. Geol.* **2008**, *257*, 34–43. [CrossRef]
59. Ludwig, K.R. ISOPLOT 3.00: A Geochronological Toolkit for Microsoft Excel. *Calif.: Berkeley Geochronol. Cent.* **2003**, *4*, 67.
60. Hu, Z.C.; Liu, Y.S.; Gao, S.; Liu, W.G.; Zhang, W.; Tong, X.R.; Lin, L.; Zong, K.Q.; Li, M.; Chen, H.H. Improved in Situ Hf Isotope Ratio Analysis of Zircon Using Newly Designed X Skimmer Cone and Jet Sample Cone in Combination with the Addition of Nitrogen by Laser Ablation Multiple Collector ICP-MS. *J. Anal. Atom. Spectrom.* **2012**, *27*, 1391–1399. [CrossRef]
61. Liu, Y.S.; Gao, S.; Hu, Z.C.; Gao, C.G.; Zong, K.Q.; Wang, D.B. Continental and Oceanic Crust Recycling-Induced Melt-Peridotite Interactions in the Trans-North China Orogen: U-Pb Dating, Hf Isotopes and Trace Elements in Zircons from Mantle Xenoliths. *J. Petrol.* **2010**, *51*, 537–571. [CrossRef]
62. Blichert-Toft, J.; Albarède, F. The Lu-Hf Isotope Geochemistry of Chondrites and the Evolution of the Mantle-Crust System. *Earth Planet. Sci. Lett.* **1997**, *148*, 243–258. [CrossRef]
63. McCulloch, M.T.; Rosman, K.J.R.; De Laeter, J.R. The Isotopic and Elemental Abundance of Ytterbium in Meteorites and Terrestrial Samples. *Geochim. Cosmochim. Acta* **1977**, *41*, 1703–1707. [CrossRef]
64. Blichert-Toft, J.; Chauvel, C.; Albarède, F. Separation of Hf and Lu for Highprecision Isotope Analysis of Rock Samples by Magnetic Sector-Multiple Collector ICP-MS. *Contrib. Mineral. Petrol.* **1997**, *127*, 248–260. [CrossRef]
65. Vermeesch, P. On the Visualisation of Detrital Age Distributions. *Chem. Geol.* **2012**, *312*, 190–194. [CrossRef]
66. Spencer, C.J.; Kirkland, C.L.; Taylor, R.J.M. Strategies Towards Statistically Robust Interpretations of in Situ U–Pb Zircon Geochronology. *Geosci. Front.* **2016**, *7*, 581–589. [CrossRef]
67. Wang, W.; Zhou, M.F.; Yan, D.P.; Li, J.W. Depositional Age, Provenance, and Tectonic Setting of the Neoproterozoic Sibao Group, Southeastern Yangtze Block, South China. *Precambrian Res.* **2012**, *192–195*, 107–124. [CrossRef]
68. Meng, Q.X.; Zhang, J.; Geng, J.Z.; Zhang, C.L.; Huang, W.C. Zircon U–Pb age and Hf Isotope Compositions of the Lengjiaxi and Banxi Groups in Middle Hunan Province: Implications for the Neoproterozoic Tectonic Evolution in South China. *Geol. China* **2013**, *1*, 191–216. (In Chinese with English abstract)
69. Wang, J.Q.; Shu, L.S.; Santosh, M. U-Pb and Lu-Hf Isotopes of Detrital Zircon Grains from Neoproterozoic Sedimentary Rocks in the Central Jiangnan Orogen, South China: Implications for Precambrian Crustal Evolution. *Precambrian Res.* **2017**, *294*, 175–188. [CrossRef]
70. Wang, P.M.; Yu, J.H.; Sun, T.; Ling, H.F.; Chen, P.R.; Zhao, K.D.; Chen, W.F.; Liu, Q. Geochemistry and Detrital Zircon Geochronology of Neoproterozoic Sedimentary Rocks in Eastern Hunan Province and Their Tectonic Significance. *Acta Petrol. Sin.* **2012**, *28*, 3841–3857.
71. Wang, D.; Wang, X.L.; Zhou, J.C.; Shu, X.J. Unraveling the Precambrian Crustal Evolution by Neoproterozoic Conglomerates, Jiangnan Orogen: U–Pb and Hf Isotopes of Detrital Zircons. *Precambrian Res.* **2013**, *233*, 223–236. [CrossRef]
72. Yan, C.L.; Shu, L.S.; Santosh, M.; Yao, J.L.; Li, J.Y.; Li, C. The Precambrian Tectonic Evolution of the Western Jiangnan Orogen and Western Cathaysia Block: Evidence from Detrital Zircon Age Spectra and Geochemistry of Clastic Rocks. *Precambrian Res.* **2015**, *268*, 33–60. [CrossRef]
73. Liu, X.M.; Gao, S.; Diwu, C.R.; Ling, W.L. Precambrian Crustal Growth of Yangtze Craton as Revealed by Detrital Zircon Studies. *Am. J. Sci.* **2008**, *308*, 421–468. [CrossRef]
74. Wang, L.J.; Griffin, W.L.; Yu, J.H.; O'Reilly, S.Y. Precambrian Crustal Evolution of the Yangtze Block Tracked by Detrital Zircons from Neoproterozoic Sedimentary Rocks. *Precambrian Res.* **2010**, *177*, 131–144. [CrossRef]
75. Wang, W.; Chen, F.K.; Hu, R.; Chu, Y.; Yang, Y.Z. Provenance and Tectonic Setting of Neoproterozoic Sedimentary Sequences in the Southchina Block: Evidence from Detrital Zircon Ages and Hf–Nd Isotopes. *Int. J. Earth Sci.* **2012**, *101*, 1723–1744. [CrossRef]
76. Wang, X.C.; Li, X.H.; Li, Z.X.; Li, Q.L.; Tang, G.Q.; Gao, Y.Y.; Zhang, Q.R.; Liu, Y. Episodic Precambrian Crust Growth: Evidence from U-Pb Ages and Hf-O Isotopes of Zircon in the Nanhua Basin, Central South China. *Precambrian Res.* **2012**, *222–223*, 386–403. [CrossRef]
77. Dai, C.G.; Chen, J.S.; Lu, D.B.; Ma, H.Z.; Wang, X.H. Wuling Orogeny in Eastern Guizhou and Its Adjacent Regions and Its Geological Significance. *J. Geomech.* **2010**, *16*, 78–85. (In Chinese with English abstract)
78. BGMRHN. *Regional Geological Survey Report (Liuyang Area, 1:200,000)*; BGMRHN: Hunan, China, 1976. (In Chinese)
79. BGMRHN. *Regional Geological Survey Report (Pingjiang Area, 1:200,000)*; BGMRHN: Hunan, China, 1977. (In Chinese)
80. BGMRHN. *Regional Geological Survey Report (Qianyang Area, 1:50,000)*; BGMRHN: Hunan, China, 2000. (In Chinese)
81. Zhang, S.H.; Jiang, G.Q.; Dong, J.; Han, Y.G.; Wu, H.C. New SHRIMP U-Pb Age from the Wuqiangxi Formation of Banxi Group: Implications for Rifting and Stratigraphic Erosion Associated with the Early Cryogenian (Sturtian) Glaciation in South China. *Sci. China Ser. D Earth. Sci.* **2008**, *51*, 1537–1544. [CrossRef]
82. Lan, Z.W.; Li, X.H.; Zhu, M.Y.; Zhang, Q.R.; Li, Q.L. Revisiting the Liantuo Formation in Yangtze Block, South China: Sims U-Pb Zircon Age Con-Straints and Regional and Global Significance. *Precambrian Res.* **2015**, *263*, 123–141. [CrossRef]

83. Yin, C.Y.; Liu, D.Y.; Gao, L.Z.; Wang, Z.Q.; Xing, Y.S.; Jian, P.; Shi, Y.R. Lower Boundary Age of the Nanhua Systemand Thegucheng Glacial Stage: Evidence from SHRIMP II Dating. *Chin. Sci. Bull* **2003**, *48*, 1657–1662. [CrossRef]
84. Dickinson, W.R.; Gehrels, G.E. Use of U-Pb Ages of Detrital Zircons to Infer Maximum Depositional Ages of Strata: A Test against a Colorado Plateau Mesozoic Database. *Earth Planet. Sci. Lett.* **2009**, *288*, 115–125. [CrossRef]
85. Gao, L.Z.; Chen, J.S.; Dai, C.G.; Ding, X.Z.; Wang, X.H.; Liu, Y.X.; Min, W.; Zhang, H. SHRIMP Zircon U-Pb Dating of Tuff in Fanjingshan Group and Xiajiang Group from Guizhou and Hunan Provinces and Its Stratigraphic Implications. *Geol. Bull. China* **2014**, *33*, 949–959. (In Chinese with English abstract)
86. Gao, L.Z.; Chen, J.; Ding, X.Z.; Liu, Y.R.; Zhang, C.H.; Zhang, H.; Liu, Y.X.; Pang, W.H.; Zhang, Y.H. Zircon SHRIMP U-Pb Dating of the Tuff Bed of Lengjiaxi and Banxi Groups, Northeastern Hunan: Constraints on the Wuling Movement. *Geol. Bull. China* **2011**, *30*, 1001–1008. (In Chinese with English abstract)
87. Gao, L.Z.; Dai, C.G.; Liu, Y.X.; Wang, M.; Wang, X.H.; Chen, J.S.; Ding, X.Z. Zircon SHRIMP U-Pb Dating of the Tuffaceous Bed of Xiajiang Group in Guizhou Province and Its Stratigraphic Implication. *Geol. China* **2010**, *37*, 1071–1080. (In Chinese with English abstract)
88. Du, Q.D.; Wang, Z.J.; Wang, J.; Qiu, Y.S.; Jiang, X.S.; Deng, Q.; Yang, F. Geochronology and Paleoenvironment of the Pre-sturtian Glacial Strata: Evidence from the Liantuo Formatin in the Nanhua Rift Basin of the Yangtze Block, South China. *Precambrian Res.* **2013**, *233*, 118–131. [CrossRef]
89. Ma, G.G.; Li, H.Q.; Zhang, Z.C. An Investigation of the Age Limits of the Sinian System in South China. *Geol. Sci.* **1984**, *8*, 1–29.
90. Sun, H.Q.; Huang, J.Z.; Guo, L.Q.; Chen, J. Subdivision and Isotopic Age of Lengjiaxi Group in Hunan Province. *Geol. Miner. Resour. South China* **2012**, *28*, 20–26. (In Chinese with English abstract)
91. Zhang, Q.R.; Li, X.H.; Feng, L.J.; Huang, J.; Song, B. A New Age Constraint on the Onset of the Neoproterozoic Glaciations in the Yangtze Platform, South China. *J. Geol.* **2008**, *116*, 423–429. [CrossRef]
92. Liu, S.L.; Cui, X.Z.; Wang, C.L.; Ren, G.M.; Ren, F.; Chen, F.L. Zircon U-Pb Geochronological Study of the Pinglue Formation Tuffite and Its Geological Significance, Southeast Guizhou Province. *Mineral. Petrol.* **2020**, *40*, 21–27. (In Chinese with English abstract)
93. Lan, Z.W.; Li, X.H.; Zhu, M.Y.; Chen, Z.Q.; Zhang, Q.R.; Li, Q.L.; Lu, D.B.; Liu, Y.; Tang, G.Q. A Rapid and Synchronous Initiation of the Sturtian Glaciations. *Precambrian Res.* **2014**, *255*, 401–411. [CrossRef]
94. Gao, L.Z.; Lu, J.P.; Ding, X.Z.; Wang, H.R.; Liu, Y.X.; Li, J. Zircon U-Pb Dating of Neoproterozoic Tuff in South Guangxi and Its Implications for Stratigraphic Correlation. *Geol. China* **2013**, *40*, 1443–1452. (In Chinese with English abstract)
95. Zhou, J.C.; Wang, X.L.; Qiu, J.S. Geochronology of Neoproterozoic Mafic Rocks and Sandstones from Northeastern Guizhou, South China: Coeval Arc Magmatism and Sedimentation. *Precambrian Res.* **2009**, *170*, 27–42. [CrossRef]
96. Su, J.B.; Dong, S.W.; Zhang, Y.Q.; Li, Y.; Chen, X.H.; Cui, J.J. Detrital Zircon Geochronology of Pre-cretaceous Strata: Tectonic Implications for the Jiangnan Orogen, South China. *Geol. Mag.* **2014**, *151*, 975–995. [CrossRef]
97. Zhang, Y.Z.; Wang, Y.J.; Zhang, Y.H.; Zhang, A.M. Neoproterozoic Assembly of the Yangtze and Cathaysia Blocks: Evidence from the Cangshuipu Group and Associated Rocks along the Central Jiangnan Orogen, South China. *Precambrian Res.* **2015**, *269*, 18–30. [CrossRef]
98. Wang, X.L.; Zhou, J.C.; Qiu, J.S.; Zhang, W.L.; Liu, X.M.; Zhang, G.L. LA-ICP-MS U-Pb Zircon Geochronology of the Neoproterozoic Igneous Rocks from Northern Guangxi, South China: Implications for Tectonic Evolution. *Precambrian Res.* **2006**, *145*, 111–130. [CrossRef]
99. Zhou, J.B.; Li, X.H.; Ge, W.C.; Li, Z.X. Age and Origin of Middle Neoproterozoic Mafic Magmatism in Southern Yangtze Block and Relevance to the Break-up of Rodinia. *Gondwana Res.* **2007**, *12*, 184–197. [CrossRef]
100. Chen, Z.H.; Guo, K.Y.; Dong, Y.G.; Chen, R.; Li, L.M.; Liang, Y.H.; Li, C.H.; Yu, X.M.; Zhao, L.; Xing, G.F. Possible Early Neoproterozoic Magmatism Associated with Slab Window in the Pingshui Segment of the Jiangshan-Shaoxing Suture Zone: Evidence from Zircon LA-ICP-MS U-Pb Geochronology and Geochemistry. *Sci. China Ser. D Earth. Sci.* **2009**, *52*, 925–939. [CrossRef]
101. Fan, Q.C.; Zhang, C.H.; You, G.Q.; Dong, L.L.; Liu, D.B.; Lu, C.M. Sedimentary Features and Basin Prototype of Fanjingshan Group. *Acta Geosci. Sin.* **2017**, *38*, 513–522. (In Chinese with English abstract)
102. Greentree, M.R.; Li, Z.X. The Oldest Known Rocks in South-Western China: SHRIMP U-Pb Magmatic Crystallisation Age and Detrital Provenance Analysis of the Paleoproterozoic Dahongshan Group. *J. Asian Earth Sci.* **2008**, *33*, 289–302. [CrossRef]
103. Zhao, X.F.; Zhou, M.F.; Li, J.W.; Sun, M.; Gao, J.F.; Sun, W.H.; Yang, J.H. Late Paleoproterozoic to Early Mesoproterozoic Dongchuan Group in Yunnan, SW China: Implications for Tectonic Evolution of the Yangtze Block. *Precambrian Res.* **2010**, *182*, 57–69. [CrossRef]
104. Wang, W.; Zhou, M.F. Provenance and Tectonic Setting of the Paleo– To Mesoproterozoic Dongchuan Group in the Southwestern Yangtze Block, South China: Implication for the Breakup of the Supercontinent Columbia. *Tectonophysics* **2014**, *610*, 110–127. [CrossRef]
105. Zhang, S.B.; Zheng, Y.F.; Wu, Y.B.; Zhao, Z.F.; Gao, S.; Wu, F.Y. Zircon U–Pb age and Hf–O Isotope Evidence for Paleoproterozoic Metamorphic Event in South China. *Precambrian Res.* **2006**, *151*, 265–288. [CrossRef]
106. Sun, M.; Chen, N.S.; Zhao, G.C.; Wilde, S.A.; Ye, K.; Guo, J.H.; Chen, Y.; Yuan, C. U–Pb Zircon and SM–ND Isotopic Study of the Huangtuling Granulite, Dabie–Sulu Belt, China: Implication for the Paleoproterozoic Tectonic History of the Yangtze Craton. *Am. J. Sci.* **2008**, *308*, 469–483. [CrossRef]

107. Xiong, Q.; Zheng, J.P.; Yu, C.; Su, Y.; Tang, H.; Zhang, Z. Zircon U–Pb Age and Hf Isotope of Quanyishang A-Type Granite in Yichang: Signification for the Yangtze Continental Cratonization in Paleoproterozoic. *Chin. Sci. Bull.* **2009**, *54*, 436–446. [CrossRef]
108. Wu, Y.B.; Gao, S.; Zhang, H.; Zheng, J.P.; Liu, X.; Wang, H.; Gong, H.; Zhou, L.; Yuan, H. Geochemistry and Zircon U–Pb Geochronology of Paleoproterozoic Arc Related Granitoid in the Northwestern Yangtze Block and Its Geological Implications. *Precambrian Res.* **2012**, *200*, 26–37. [CrossRef]
109. Yin, C.Q.; Lin, S.F.; Davis, D.W.; Zhao, G.C.; Xiao, W.J.; Li, L.M.; He, Y.H. 2.1–1.85 GA Tectonic Events in the Yangtze Block, South China: Petrological and Geochronological Evidence from the Kongling Complex and Implications for the Reconstruction of Supercontinent Columbia. *Lithos* **2013**, *182*, 200–210. [CrossRef]
110. Yang, Z.N.; Yang, K.G.; Xu, Y.; Deng, X.; Cheng, W.Q.; Long, Z.Y. Zircon U-Pb Geochronology, Hf Isotopic Composition, and Geological Implications of the Neoproterozoic Meta-Sedimentary Rocks in Suizhou-Zaoyang Area, the Northern Yangtze Block. *Sci. China Earth. Sci.* **2015**, *58*, 1910–1923. [CrossRef]
111. Li, Y.H.; Zheng, J.P.; Xiong, Q.; Wang, W.; Ping, X.Q.; Li, X.Y.; Tang, H.Y. Petrogenesis and Tectonic Implications of Paleoproterozoic Metapelitic Rocks in the Archean Kongling Complex from the Northern Yangtze Craton, South China. *Precambrian Res.* **2016**, *276*, 158–177. [CrossRef]
112. Nie, H.; Yao, J.; Wan, X.; Zhu, Y.X.; Siebel, W.; Chen, F.K. Precambrian Tectonothermal Evolution of South Qinling and Its Affinity to the Yangtze Block: Evidence from Zircon Ages and Hf–Nd Isotopic Compositions of Basement Rocks. *Precambrian Res.* **2016**, *286*, 167–179. [CrossRef]
113. Han, Q.S.; Peng, S.B.; Polat, A.; Kusky, T. Petrogenesis and Geochronology of Paleoproterozoic Magmatic Rocks in the Kongling Complex: Evidence for a Collisional Orogenic Event in the Yangtze Craton. *Lithos* **2019**, *342*, 513–529. [CrossRef]
114. Li, Q.W.; Zhao, J.H.; Wang, W. Ca. 2.0 Ga Mafic Dikes in the Kongling Complex, South China: Implications for the Reconstruction of Columbia. *J. Asian Earth Sci.* **2019**, *169*, 323–335. [CrossRef]
115. Wu, Y.B.; Chen, D.G.; Xia, Q.K.; Deloule, E.; Chen, H. SIMS U–Pb Dating of Zircons in Granulite of Huangtuling from Northern Dabieshan. *Acta Petrol. Sin.* **2002**, *18*, 378–382. (In Chinese with English abstract)
116. Hu, J.; Liu, X.C.; Chen, L.Y.; Qu, W.; Li, H.K.; Geng, J.Z. A _2.5 Ga Magmatic Event at the Northern Margin of the Yangtze Craton: Evidence from U-Pb Dating and Hf Isotope Analysis of Zircons from the Douling Complex in the South Qinling Orogen. Chin. *Sci. Bull.* **2013**, *58*, 3564–3579. [CrossRef]
117. Wu, Y.B.; Zhou, G.Y.; Gao, S.; Liu, X.C.; Qin, Z.W.; Wang, H.; Yang, J.Z.; Yang, S.H. Petrogenesis of Neoarchean TTG Rocks in the Yangtze Craton and Its Implication for the Formation of Archean TTGs. *Precambrian Res.* **2014**, *254*, 73–86. [CrossRef]
118. Chen, K.; Gao, S.; Wu, Y.B.; Guo, J.L.; Hu, Z.C.; Liu, Y.S.; Zong, K.Q.; Liang, Z.W.; Geng, X.L. 2.6-2.7 Ga Crustal Growth in Yangtze Craton, South China. *Precambrian Res.* **2013**, *224*, 472–490. [CrossRef]
119. Guo, J.L.; Wu, Y.B.; Gao, S.; Jin, Z.M.; Zong, K.Q.; Hu, Z.C.; Chen, K.; Chen, H.H.; Liu, Y.S. Episodic Paleoarchean-Paleoproterozoic (3.3–2.0 Ga) Granitoid Magmatism in Yangtze Craton, South China: Implications for late Archean Tectonics. *Precambrian Res.* **2015**, *270*, 246–266. [CrossRef]
120. Wang, Z.J.; Wang, J.; Du, Q.D.; Deng, Q.; Yang, F.; Wu, H. Mature Archean Continental Crust in the Yangtze Craton: Evidence from Petrology, Geochronology and Geochemistry. *Chin. Sci. Bull.* **2013**, *58*, 2360–2369. [CrossRef]
121. Zhou, G.Y.; Wu, Y.B.; Gao, S.; Yang, J.Z.; Zheng, J.P.; Qin, Z.W.; Wang, H.; Yang, S.H. The 2.65 Ga A-type Granite in the Northeastern Yangtze Craton: Petrogenesis and Geological Implications. *Precambrian Res.* **2015**, *258*, 247–259. [CrossRef]
122. Zhang, S.B.; Zheng, Y.F.; Wu, Y.B.; Zhao, Z.F.; Gao, S.; Wu, F.Y. Zircon U-Pb Age and Hf Isotope Evidence for 3.8 Ga Crustal Remnant and Episodic Reworking of Archean Crust in South China. *Earth Planet. Sci. Lett.* **2006**, *252*, 56–71. [CrossRef]
123. Liu, Y.; Yang, K.G.; Polat, A.; Ma, X. Reconstruction of the Cryogenian Palaeogeography in the Yangtze Domain: Constraints from Detrital Age Patterns. *Geol. Mag.* **2019**, *156*, 1247–1264. [CrossRef]
124. Wei, Y.N.; Jiang, X.S.; Cui, X.Z.; Zhuo, J.W.; Jiang, Z.F.; Cai, J.J. Detrital Zircon U–Pb Ages of the Neoproterozoic Qingshuijiang Formation in Southeastern Guizhou and Their Geological Significance. *Mineral. Petrol.* **2015**, *35*, 61–71. (In Chinese with English abstract)
125. Zhang, C.L.; Santosh, M.; Zou, H.B.; Li, H.K.; Huang, W. The Fuchuan Ophiolite in Jiangnan Orogen: Geochemistry, Zircon U-Pb Geochronology, Hf Isotope and Implications for the Neoproterozoic Assembly of South China. *Lithos* **2013**, *179*, 263–274. [CrossRef]
126. Wu, R.X.; Zheng, Y.F.; Wu, Y.B.; Zhao, Z.F.; Zhang, S.B.; Liu, X.M.; Wu, F.Y. Reworking of Juvenile Crust: Element and Isotope Evidence from Neoproterozoic Granodiorite in South China. *Precambr Res.* **2006**, *146*, 179–212. [CrossRef]
127. Wang, X.L.; Shu, L.S.; Xing, G.F.; Zhou, J.C.; Tang, M.; Shu, X.; Qi, L.; Hu, Y.H. Post-orogenic Extension in the Eastern Part of the Jiangnan Orogen: Evidence from ca 800–760 Ma Volcanic Rocks. *Precambrian Res.* **2012**, *222–223*, 404–423. [CrossRef]
128. Zhang, S.B.; Wu, F.Y.; Zheng, Y.F. Neoproterozoic Continental Accretion in South China: Geochemical Evidence from the Fuchuan Ophiolite in the Jiangnan Orogeny. *Precambrian Res.* **2012**, *220–221*, 45–64. [CrossRef]
129. Dong, Y.P.; Sun, S.S.; Yang, Z.; Liu, X.M.; Zhang, F.F.; Li, W.; Cheng, B.; He, D.F.; Zhang, G.W. Neoproterozoic Subduction-Accretionary Tectonics of the South Qinling Belt, China. *Precambrian Res.* **2017**, *293*, 73–90. [CrossRef]
130. Deng, Q.; Wang, J.; Wang, Z.J.; Wang, X.C.; Qiu, Y.S.; Yang, Q.X.; Du, Q.D.; Cui, X.Z.; Zhou, X.L. Continental Flood Basalts of the Huashan Group, Northern Margin of the Yangtze Block—Implications for the Breakup of Rodinia. *Int. Geol. Rev.* **2013**, *55*, 1865–1884. [CrossRef]

131. Huang, Y.; Wang, X.L.; Li, J.Y.; Wang, D.; Chang-Hong Jiang, C.H.; Li, L.S. Early Neoproterozoic Tectonic Evolution of Northern Yangtze Block: Insights from Sedimentary Sequences from the Dahongshan Area. *Precambrian Res.* **2021**, *365*, 106382. [CrossRef]
132. Hu, J.; Liu, X.C.; Qu, W.; Chen, L.Y. Mid-Neoproterozoic Amphibolite Facies Metamorphism at the Northern Margin of the Yangtze Craton. *Precambrian Res.* **2019**, *326*, 333–343. [CrossRef]
133. Pei, X.Z.; Li, Z.C.; Ding, S.P.; Li, R.B.; Feng, J.Y.; Sun, Y.; Zhang, Y.F.; Liu, Z.Q. Neoproterozoic Jiaoziding Peraluminous Granite in the Northwestern Margin of Yangtze Block: Zircon SHRIMP U-Pb Age and Geochemistry and Their Tectonic Significance. *Earth Sci. Front.* **2009**, *16*, 231–249. [CrossRef]
134. Wang, H.Z.; Laurent, O.; Zhang, H.F.; Zhang, H.; Chen, X.; Zhai, M.G. Recognition and Significance of C. 800 Ma Upper Amphibolite to Granulite Facies Metamorphism in Metasedimentary Rocks from the NW Margin of the Yangtze Block. *J. Geol. Soc.* **2020**, *177*, 424–441.